AD NUMBER
AD119103
LIMITATION CHANGES
TO: **Approved for public release; distribution is unlimited.**
FROM: **Distribution authorized to U.S. Gov't. agencies and their contractors; Administrative/Operational Use; 21 NOV 1956. Other requests shall be referred to U.S. Naval Ordnance Laboratory, White Oak, MD.**
AUTHORITY
USNOL ltr dtd 29 Aug 1974

NAVORD REPORT 4339

FC

A STUDY OF BOUNDARY-LAYER TRANSITION FROM LAMINAR TO TURBULENT FLOW

21 NOVEMBER 1956

DEPARTMENT OF THE NAVY
NAVAL ORDNANCE LABORATORY

U. S. NAVAL ORDNANCE LABORATORY

WHITE OAK, MARYLAND

NAVORD Report 4339

Aeroballistic Research Report 349

A STUDY OF BOUNDARY-LAYER TRANSITION FROM LAMINAR TO TURBULENT FLOW

Prepared by:

Jerome Persh

ABSTRACT: A large amount of boundary-layer data in the region of transition from laminar to turbulent flow has been collected from a number of experimental investigations of boundary-layer flows on flat plates, circular cylinders, and airfoils. These data are for both incompressible and compressible flows without heat transfer.

The criterion for determining the axial position of the beginning and end of transition proposed by the author in reference (a) is verified by examination of a large amount of experimental data. Comparisons are given between the experimental values of several boundary-layer parameters at the start of transition and the theoretical values predicted by the modified (reference b) stability theory of Schlichting and Ulrich (reference c). It is shown that for incompressible flows, the start of transition may be roughly predicted by stability theory. This is demonstrated by comparisons between a number of zero pressure gradient and pressure gradient examples.

U. S. NAVAL ORDNANCE LABORATORY
WHITE OAK, MARYLAND

NAVORD Report 4339 21 November 1956

This report contains the results of a preliminary investigation of the mechanics of the boundary-layer transition process. From an examination of a large amount of experimental boundary-layer velocity profile data on flat plates, circular cylinders, and airfoils in both subsonic and supersonic airstreams. Several significant conclusions are drawn. This study is important at the present time because probably the weakest link in the calculation of wall temperatures and heat transfer to missiles is the determination of the transition region.

This work was sponsored by the U. S. Navy Bureau of Ordnance and was performed under Task Number NOL M9a-133-1-56. The author is indebted to Dr. R. E. Wilson and Dr. R. K. Lobb for their encouragement and continued interest during the course of the investigation.

WILLIAM W. WILBOURNE
Captain, USN
Commander

H. H. KURZWEG
By direction

CONTENTS

	Page
Introduction	1
Review of Experimental Investigations.	1
Zero Pressure Gradient Data	2
Pressure Gradient Data.	2
Evaluation and Presentation of Data.	3
Discussion of Results.	3
Correlation of the Boundary-Layer Parameters at the Start of Transition	4
Incompressible Flows.	4
Compressible Flows	5
Correlation of Boundary-Layer Velocity Profile Data. .	5
Concluding Remarks	6
References	7
Table I.	9
Table II	12
Table III.	19
Table IV	22

ILLUSTRATIONS

Figure 1. Variation of H with distance along flat plate. Data of reference d.

Figure 2. Variation of H with distance along flat plate. Data of reference e.

Figure 3. Variation of H_{inc} with distance along circular cylinder in axial flow at M = 2.41. Data of reference f.

Figure 4. Variation of H_{inc} with distance along circular cylinder in axial flow at M = 3.05. Data of reference g.

Figure 5. Variation of H with distance along NACA 0009 airfoil. Data of reference h.

Figure 6. Variation of H with distance along NACA 0012 airfoil. Data of reference h.

Figure 7. Variation of H with distance along NACA 0018 airfoil. Data of reference h.

Figure 8. Variation of H with distance along symmetrical Joukowski airfoil. Data of reference i.

Figure 9. Comparison between the theoretical values of $R_{\theta_{cr.min}}$ and experimental data as a function of $R_\theta \ \theta/u_\infty \ du_\infty/dx$ for incompressible flow data.

Figure 10. Comparison between theoretical values of $H_{cr.}$ and experimental data as a function of $R_\theta \ \theta/u_\infty \ du_\infty/dx$ for incompressible flow data.

Figure 11. Variation of $R_{\theta T_r}$ with Mach number for compressible flow data.

Figure 12. Variation of $R_{\theta T_r}$ with supply pressure for compressible flow data.

Figure 13. Correlation of transition region velocity profile data.

SYMBOLS

H	- boundary-layer shape parameter (δ^*/θ)
M	- Mach number
P_o	- stagnation pressure
q	- dynamic pressure outside the boundary layer $(1/2 \rho_\infty U_\infty^2)$
R_θ	- boundary-layer Reynolds number based on momentum thickness $(U_\infty \theta / \nu_\infty)$
u	- velocity parallel to surface at a perpendicular distance y from wall
U_∞	- velocity parallel to surface at a distance δ from wall
x	- longitudinal distance from leading edge of flat plate or circular cylinder
s	- longitudinal distance from leading edge of airfoil measured along surface
y	- perpendicular distance from wall to point at which velocity u is measured
δ	- boundary-layer thickness, defined as perpendicular distance from wall to point at which contribution to the integrals for δ^* and θ is negligible
δ^*	- boundary-layer displacement thickness for incompressible flow

$$\int_0^\delta \left(1 - \frac{u}{U_\infty}\right) dy$$

δ^*_{comp}	- boundary-layer displacement thickness for compressible flow

$$\int_0^\delta \left(1 - \frac{\rho u}{\rho_\infty U_\infty}\right) dy$$

θ - boundary-layer momentum thickness for incompressible flow

$$\int_0^{\delta} \frac{u}{U_\infty} \left(1 - \frac{u}{U_\infty}\right) dy$$

θ_{comp} - boundary-layer momentum thickness for compressible flow

$$\int_0^{\delta} \frac{\rho\, u}{\rho_\infty U_\infty} \left(1 - \frac{u}{U_\infty}\right) dy$$

μ - viscosity

ρ - density

ν - kinematic viscosity,

c_f - wall shear stress coefficient (τ_w/q)

Subscripts:

inc - incompressible flow

comp - compressible flow

exp - experimental

Tr - experimental transition value

When values of δ^*, θ, H, and R_θ are not subscripted, the incompressible and experimental values of these parameters are inferred.

A STUDY OF BOUNDARY-LAYER TRANSITION FROM LAMINAR TO TURBULENT FLOW

INTRODUCTION

1. The study of boundary-layer transition from laminar to turbulent flow involves not only the determination of the factors which control the occurrence of transition, but also the changes that the boundary-layer velocity profile undergoes while reverting from wholly laminar flow to fully turbulent flow. Although a great deal of theoretical and experimental work has been done on transition, very little is known of the behavior of the boundary layer in the transition region.

2. To the author's knowledge, no theoretical work on the behavior of the boundary layer in the transition region has been done. The present work deals with both aspects of the problem. From an examination of a large amount of velocity profile and pressure distribution data taken from a number of experimental investigations of flat plates, hollow cylinder models, and airfoils in both incompressible and compressible flows, it is shown that the criterion for determining the axial location of the start of transition proposed by the author in reference (a) is substantiated. It is also shown that for incompressible flows with moderate values of stream turbulence, roughness, or pressure gradient, the start of transition may be roughly predicted by stability theory.

REVIEW OF EXPERIMENTAL INVESTIGATIONS

3. While it is realized that the published results of a number of experimental investigations, in addition to the results presented herein, are available, the data presented were drawn from those investigations that were most suited to the present work and it is felt that the results shown are representative of the entire fund of information. It should be noted that only the general features of each investigation can be discussed in the present report and it is suggested that the reader consult the original papers for more detailed information.

4. For convenience, the results of the experimental investigations have been separated into two categories, namely, the zero pressure gradient cases (flat plate and hollow cylinder models) and the cases for which pressure gradients existed (airfoils). In order that the data presented be as complete as possible, the values of stream turbulence when available, are given in the tables presented.

Zero Pressure Gradient Data

5. The pioneer measurements of the boundary-layer flow on a flat plate were made by van der Hegge Zijnen (reference d) with the aid of a hot-wire anemometer. The results are presented in the form of numerous tables and curves giving the observed speeds at several hundred points, whose x and y coordinates with respect to the leading edge of the plate are tabulated for five subsonic speeds of the approaching airstream. All the results of this investigation are included in the present report in both graphical and tabular form (Table I).

6. Also included in this table are results obtained during the course of an experimental investigation of the boundary-layer flow on a flat plate made at the National Bureau of Standards by Schubauer and Klebanoff (reference e). These data were obtained at a free-stream velocity of about 80 feet/second.

7. The results of experimental investigations of the boundary-layer development on hollow cylinder models conducted by O'Donnell and Brinich and Diaconis (references f and g) with their axes aligned parallel to the airstream at Mach numbers of 2.41 and 3.05 are presented graphically and are tabulated in Table II. Results are given for four model diameters (1.87, 3, 4, and 5 inches). Only the natural transition results for these models are presented.

Pressure Gradient Data

8. The results of an experimental investigation of boundary-layer transition on three symmetrical airfoil sections, each at three angles of attack, presented by Silverstein and Becker (reference h) are given graphically and in Table III. In these tests, boundary-layer velocity profiles were measured on the upper surfaces of airfoils of the NACA 0009, 0012, and 0018 sections over a lift coefficient range from -0.57 to 0.65. Although tests were made at tunnel velocities from 30 to 90 miles per hour, only those data at 60 miles per hour are included in the present work because these are typical of all the data included in this reference.

9. The results of an experimental investigation of the boundary-layer flow on a symmetrical Joukowski airfoil section presented by Fage and Falkner (reference i) are illustrated and are also tabulated in Table IV. For this experiment a series of boundary-layer velocity profile measurements were made on the airfoil surface at tunnel airspeeds of 60 and 80 feet per second.

EVALUATION AND PRESENTATION OF DATA

10. For all of the boundary-layer velocity profile data accumulated, values of the displacement thickness (δ^*), momentum thickness (θ), and boundary-layer shape parameter (H) were evaluated by graphical integration. It has been pointed out (reference j) that compressible boundary-layer velocity profiles are similar in shape to incompressible velocity profiles. The values of parameters derived from the compressible boundary-layer velocity profiles, ignoring the temperature distribution across the boundary layer, are therefore close to those for incompressible flow. These values of the boundary-layer parameters are ficticious in a sense, but their use provides a common basis for comparisons between the results for incompressible and compressible flows. For the compressible flow data the boundary-layer parameters were therefore evaluated using both the incompressible and compressible flow definitions. Each of the tabulated sets of data are identified by the conditions of the experiment and the reference letter.

11. For the pressure gradient data investigated, the values of the stability parameter (reference b)

$$R_\theta \frac{\theta}{u_\infty} \frac{du_\infty}{dx} = \frac{\theta^2}{\nu_\infty} \frac{du_\infty}{dx} \tag{1}$$

are also tabulated. These values were calculated from the pressure distribution graphs given in the pertinent references.

DISCUSSION OF RESULTS

12. The large mass of experimental data presented herein are used first to give additional support to the transition criterion proposed in reference (a). In this reference it is shown that at the transition point an abrupt drop occurs in the curve showing the variation of the incompressible (or compressible) value of H with distance along the surface. This occurs because at the start of transition, the velocity gradient near the surface, or the skin friction, rises rapidly. The value of H is quite sensitive to the velocity ratios near the surface, and small increases in the velocity gradient near the wall cause a dimunition of the values of H. Since near the leading edge, the laminar flow region is characterized by values of H which are about 2.6 and in the turbulent region the values of H are about 1.4 to 1.5, the mean position for the start of transition should be readily recognizable.

13. Figures 1 to 8 show the variation of H with distance along the surface for each of the sets of data tabulated. In each of the cases shown, a more or less abrupt drop occurs

in the H curve. In some cases (Figures 1b and 1c, for example) the curves appear rounded at the transition point. These are probably more physically realistic than the curves showing the abrupt change in slope. It is reasonable to assume that the rounding is probably present for all of the data and would have been evident if more data in this region were available. In general, however, all of the curves exhibit the same characteristic behavior. These data validate the criterion proposed in reference (a) for determining the start of transition.

14. The determination of the end of transition region is more difficult because of the asymtotic nature of the curves shown in the preceding figures. Consequently, the end of transition is arbitrarily defined as the axial position where the value of H first reaches its characteristic turbulent value of 1.4 or 1.5, or where no further decrease in H is noted. This is indicated on each of the figures showing H as a function of x.

CORRELATION OF THE BOUNDARY-LAYER PARAMETERS AT THE START OF TRANSITION

Incompressible Flows

15. On each of the preceding figures, the point at which the minimum critical Reynolds number for laminar boundary-layer stability ($R_{\theta cr.min}$) is indicated as a shaded data point. The position of these points was determined by first plotting the experimental values of R_θ as a function of distance along the surface, and noting the axial position at which $R_{\theta cr.min}$ occurred. For the incompressible flow data the values of $R_{\theta cr.min}$ which were used for this procedure were obtained from the modified Schlichting analysis of reference (b). The ordinate value for the shaded data points was determined as the value of $H_{cr.}$ associated with the value of $R_{\theta cr.min}$. An examination of Figure 1 indicated that, in general, the start of transition occurs close to $R_{\theta cr.min}$; this is more clearly illustrated in Figure 9. In this figure the experimental values of $R_{\theta tr.}$ are compared to the theoretical curve of reference (b). While there is considerable scatter in the data, which is probably due in part to insufficient data at the start of transition, it is evident that transition starts at values of R_θ which are of the same order of magnitude as those given by theory.

16. It is difficult to justify those data points which are less than $R_{\theta cr.min}$. This is because it was found in the experimental investigation of reference (e), that efforts to disturb the laminar boundary layer in the region where the Reynolds number was less than $R_{\theta cr.min}$ were unsuccessful. While the artificial distunbance created in this region was

not damped, it amplified only beyond the axial position of $R_{\theta cr.min}$. For this reason, those transition data points which fall below the theoretical value appear inconsistent, unless the turbulence level of the airstream outside the boundary layer exerts a disturbance which has characteristics different than that created artificially in the experiments of reference (e).

17. As pointed out previously, both $R_{\theta cr.min}$ and $H_{cr.}$ are uniquely defined when the value of the non-dimensional pressure gradient parameter $R_\theta \; \theta/u_\infty \; du_\infty/dx$, is specified. A comparison is shown in Figure 10 between the theoretical curve of $H_{cr.}$ and experimental values of $H_{tr.}$ as a function of $R_\theta \; \theta/u_\infty \, du_\infty/dx$. No conclusion can be drawn from this comparison because of the large data scatter. It is indicative, however, of the sensitive nature of H.

Compressible Flows

18. Figure 11 shows the values of $R_{\theta tr.}$ determined in the manner previously described for all of the compressible flow data examined. In view of the large scatter of the data, it is not possible to describe any trend with Mach number. To determine whether the transition point is a function of stagnation pressure as was suggested in reference (k), the experimental data shown in Figure 11, are plotted versus P_o in Figure 12. In this coordinate system, there seems to be some trend of increasing $R_{\theta tr.}$ with increasing stagnation pressure, but the scatter of the data is too large to draw any definite conclusions.

Correlation of Boundary-Layer Velocity Profile Data

19. From previous discussion and inspection of the related figures, it is apparent that only a small portion of the large mass of velocity profile data presented falls into the transition region. However, the data that are applicable have been isolated and are considered of sufficient quantity for the present correlation.

20. It has been shown by von Doenhoff and Tetervin (reference 1) that turbulent boundary-layer velocity profiles form a single parameter family of curves. To determine whether the transition region velocity profiles are of a single parameter family of curves, and, if so, whether the transition region velocity profiles are of the same family as those for turbulent boundary-layer velocity profiles, values of u/u_∞ were plotted against H for various values of y/θ for all the data entering into the analysis. The variation of u/u_∞ with H for several values of y/θ is shown in Figure 13. Because of the large amount of data points, and the fact that no significant

trends were detected between sets of data, no effort was made to identify the points of any one investigation. Also plotted in Figure 13 are curves of u/u_∞ versus H for corresponding values of y/θ for turbulent boundary-layer velocity profiles. Figure 13 shows that u/u_∞ is a function of H alone for a given value of y/θ. This conclusion is important because it means that transition region boundary-layer velocity profiles form single parameter family of curves. It is also apparent that the transition region velocity profiles are of a different shape than those for turbulent boundary-layer velocity profiles.

CONCLUDING REMARKS

21. A large amount of boundary-layer data in the region of transition from laminar to turbulent flow has been collected from a number of experimental investigations of boundary-layer flows on flat plates, circular cylinders, and airfoils. These data are presented in both graphical and tabular form.

22. A criterion for determining the axial position of the beginning and end of transition previously proposed in reference (a) is substantiated. Comparisons are given between the experimental values of two local boundary-layer parameters (R_θ and $\theta^2/\nu_\infty \, du_\infty/dx$) at the start of transition and the theoretical values of these parameters as predicted by stability theory. It is shown that for incompressible flows the start of transition may be roughly predicted by stability theory. No correlation between the measured values of $R_{\theta tr.}$ at the start of transition and the minimum critical values of R_θ was found for the compressible flow data.

23. It is shown that the shape of all transition region boundary-layer velocity profiles may be expressed as a function of a single parameter. It is also shown that transition region velocity profiles differ in shape from turbulent boundary-layer velocity profiles, particularly in the region near the wall.

REFERENCES

(a) Persh, Jerome, "The Behavior of the Boundary Layer in the Region of Transition From Laminar to Turbulent Flow," Jour. Aero. Sci., Vol. 22, No. 6, pp. 443-444, June 1955

(b) Tetervin, Neal and Levine, David A., "A Study of the Stability of the Laminar Boundary Layer as Affected by Changes in the Boundary-Layer Thickness in Regions of Pressure Gradient and Flow Through the Surface," NACA TN 2752, 1952

(c) Schlichting, H., and Ulrich, A., "Zur Berechnung Des Umschlages Laminar/Turbulent," Bericht S 10 der Lilienthal-Gesellschaft fur Luft Fahrtorschung, Preisausschreiben 1940, pp. 75-133

(d) van der Hegge Zijnen, B. G., "Measurements of the Velocity Distribution in the Boundary Layer along a Plane Surface," Rept. 6, Aero. Lab., Tech., H. S., Delft, 1924

(e) Schubauer, G. B., and Klebanoff, P. S., "Contributions on the Mechanics of Boundary-Layer Transition," NACA TN 3489, 1955

(f) O'Donnell, Robert M., "Experimental Investigation at a Mach Number of 2.41 of Average Skin-Friction Coefficients and Velocity Profiles for Laminar and Turbulent Boundary Layers and on Assessment of Probe Effects," NACA TN 3122, 1954

(g) Brinich, P. F., and Diaconis, N. S., "Boundary Layer Development and Skin Friction at Mach Number 3.05," NACA TN 2742, July 1952

(h) Silverstein, A., and Becker, John V., "Determination of Boundary-Layer Transition on Three Symmetrical Airfoils in the NACA Full-Scale Wind Tunnel," NACA Rept. No. 637, 1939

(i) Fage, A., and Falkner, V. M., "An Experimental Determination of the Intensity of Friction on the Surface of an Aerofoil," Aero. Res. Comm., R & M No. 1315 (Ae. 470), April 1930

(j) Persh, Jerome, "A Theoretical Investigation of Turbulent Boundary-Layer Flow with Heat Transfer at Supersonic and Hypersonic Speeds," NAVORD 3854, 1955

(k) Brinich, Paul F., "Boundary-Layer Transition at Mach 3.12 With and Without Single Roughness Elements," NACA TN 3267, 1954

(1) von Doenhoff, Albert E., and Tetervin, Neal, "Determination of General Relations for the Behavior of Turbulent Boundary Layers," NACA Rept. No. 772, 1943

TABLE I

Values of Boundary-Layer Parameters for Data of Reference d
Estimated stream turbulence 1-2 percent

U = 400 cm/sec

X, cm	δ^*, cm	θ, cm	H	R_θ
15	.1166	.04	2.915	111.9
20	.1279	.04592	2.785	125
25	.14	.0506	2.767	136.8
37.5	.1732	.0692	2.503	183.3
50	.185	.0757	2.444	206
62.5	.2166	.0976	2.22	264
75	.2422	.1129	2.145	309.3
87.5	.2464	.119	2.071	321.6
100	.2596	.1182	2.196	313
125	.2876	.133	2.162	352.3
150	.29	.1508	1.923	418.7

U = 800 cm/sec

X, cm	δ^*, cm	θ, cm	H	R_θ
5	.04624	.01992	2.321	105.6
7.5	.05744	.02344	2.451	122.7
10	.06592	.02744	2.402	145.5
12.5	.0756	.0284	2.662	149.5
15	.082	.03264	2.512	175.3
17.5	.08488	.034	2.497	179
20	.08624	.0343	2.516	184
25	.0912	.03824	2.385	207
30	.1036	.0449	2.307	243
40	.118	.0514	2.296	280
50	.1356	.0642	2.112	336
62.5	.1506	.0761	1.974	406
75	.1544	.0884	1.747	456
80	.1712	.108	1.585	576
85	.1616	.105	1.539	545
90	.1808	.12	1.507	635.5
100	.2016	.1448	1.392	777
125	.252	.182	1.385	971
150	.2992	.1536	1.948	825

TABLE I continued

U = 1200 cm/sec

X, cm	δ^*, cm	θ, cm	H	R_θ
2.5	.03368	.01684	2.0	136.5
5	.04024	.01596	2.52	127.7
7.5	.04944	.01828	2.705	144.3
10	.0553	.02036	2.715	164
15	.068	.02584	2.632	209.6
20	.07112	.02644	2.69	220.5
25	.07728	.0301	2.56	244
37.5	.0926	.0411	2.253	326.7
50	.1048	.0573	1.829	467.7
62.5	.1234	.0747	1.652	614
75	.1424	.0956	1.49	760
87.5	.1668	.1126	1.481	908
100	.2188	.1542	1.419	1210
125	.2776	.1888	1.47	1471
150	.2492	.1788	1.394	1512

U = 1600 cm/sec

X, cm	δ^*, cm	θ, cm	H	R_θ
10	.05104	.01868	2.732	196.7
15	.05768	.0232	2.486	247.6
20	.06568	.02568	2.558	274
25	.0689	.0287	2.401	304
37.5	.0758	.034	2.229	357.7
50	.0982	.0625	1.571	680
62.5	.12	.078	1.539	849
75	.1512	.0994	1.521	1075
87.5	.172	.1214	1.417	1278
100	.1852	.1312	1.412	1419
125	.2544	.1708	1.49	1872
150	.2416	.170	1.421	1890

TABLE I concluded

$U = 2400$ cm/sec

X, cm	δ^*, cm	θ, cm	H	R_θ
10	.04	.01612	2.481	254.5
15	.04432	.01844	2.403	295
20	.049	.02046	2.395	329.5
25	.05168	.0218	2.371	346.6
37.5	.05696	.03124	1.823	493.5
50	.0928	.0628	1.478	1005
62.5	.108	.0718	1.504	1142
75	.1292	.092	1.404	1473
87.5	.1496	.1064	1.406	1692
100	.1832	.1284	1.427	2069
125	.224	.1614	1.388	2619
150	.2384	.169	1.411	2836

Values of Boundary-Layer Parameters for Data of Reference e
Stream turbulence 0.03 percent

$U = 79$ ft/sec

X, ft	δ^*, in	θ, in	H	R_θ
5.00	.067	.024	2.79	924
5.25	.067	.024	2.79	928
5.75	.073	.028	2.61	1091
6.25	.060	.032	1.88	1281
6.75	.061	.041	1.49	1632
7.50	.077	.055	1.40	2180
8.00	.090	.064	1.41	2486

TABLE II

Values of Boundary-Layer Parameters for Data of Reference g M = 3.05
Stream turbulence unknown

3-inch circular cylinder p_o = 12 psia

X, in	δ^*_{inc}, in	θ_{inc}, in	H_{inc}	R_{θ} inc	δ^*_{comp}, in	θ_{comp}, in	H_{comp}	R_{θ} comp
.5	.0102	.004032	2.53	691.5	.01668	.002014	7.928	361
3.5	.02004	.007624	2.629	1308	.03176	.003752	8.465	644
6.5	.02608	.009728	2.681	1661	.04176	.00496	8.419	846.5
9.5	.02024	.01133	1.786	1931	.04216	.006496	6.49	1107
12.5	.0204	.01286	1.586	2130	.05272	.00872	6.046	1468
15.5	.028	.0184	1.522	3133	.0742	.01236	6.003	2106
18.5	.03264	.0223	1.464	3797	.08376	.01446	5.793	2461
21.5	.0396	.02784	1.422	4740	.1034	.01784	5.796	3038

3-inch circular cylinder p_o = 50 psia

X, in	δ^*_{inc}, in	θ_{inc}, in	H_{inc}	R_{θ} inc	δ^*_{comp}, in	θ_{comp}, in	H_{comp}	R_{θ} comp
.5	.008784	.002926	3.002	2033	.01327	.001493	8.888	1038
3.5	.0121	.004456	2.715	3090	.01884	.002264	8.322	1574
6.5	.0096	.006648	1.444	4622	.0254	.004336	5.858	3014
9.5	.0176	.01168	1.507	8110	.0476	.00792	6.01	5505
12.5	.01808	.01382	1.308	9600	.05024	.008736	5.751	6070
15.5	.0236	.01616	1.46	11240	.0648	.01032	6.28	7170
18.5	.02496	.0189	1.321	13140	.07288	.01206	6.043	8380
21.5	.032	.02324	1.377	16160	.0886	.01444	6.136	10040

TABLE II continued

4-inch circular cylinder p_o = 12 psia

X, in	δ^*_{inc}, in	θ_{inc}, in	H_{inc}	R_{θ} inc	δ^*_{comp}, in	θ_{comp}, in	H_{comp}	R_{θ} comp
.5	.01051	.003978	2.642	668	.01383	.002094	6.605	352
3.5	.0199	.007096	2.804	1193	.02986	.003196	9.343	537
6.5	.02072	.01005	2.062	1690	.03656	.00504	7.254	847
9.5	.01888	.01282	1.473	2155	.04748	.008032	5.911	1350
12.5	.0284	.01882	1.509	3164	.06896	.01157	5.96	1945
15.5	.03352	.02323	1.443	3904	.08432	.01432	5.888	2408
18.5	.03928	.02858	1.374	4800	.09848	.01741	5.657	2926
21.5	.0486	.03384	1.436	5690	.1162	.02092	5.555	3518

4-inch circular cylinder p_o = 50 psia

X, in	δ^*_{inc}, in	θ_{inc}, in	H_{inc}	R_{θ} inc	δ^*_{comp}, in	θ_{comp}, in	H_{comp}	R_{θ} comp
.5	.01028	.00367	2.801	2582	.0154	.001259	12.232	885.5
3.5	.0109	.006548	1.665	4609	.02376	.003256	7.297	2290
6.5	.01516	.01048	1.447	7370	.03732	.0062	6.02	4360
9.5	.02264	.01552	1.459	10920	.0532	.009264	5.743	6520
12.5	.02592	.01866	1.389	13130	.06624	.0111	5.968	7805
15.5	.02928	.02078	1.409	14610	.07392	.0127	5.821	8930
18.5	.03256	.02384	1.366	16780	.08424	.01466	5.746	10320
21.5	.04072	.02902	1.4032	20420	.09936	.01806	5.502	12710

TABLE II continued

5-inch circular cylinder p_o = 7 psia

X, in	δ^*_{inc}, in	θ_{inc}, in	H_{inc}	R_{θ} inc	δ^*_{comp}, in	θ_{comp}, in	H_{comp}	R_{θ} comp
.5	.01186	.003576	3.317	347.5	.01638	.001704	9.613	165.6
3.5	.02896	.006844	4.231	665.5	.0392	.003568	10.987	346.8
6.5	.03504	.01175	2.982	1143	.05124	.00598	8.569	581.5
9.5	.02664	.01437	1.854	1397	.05008	.008176	6.125	794
12.5	.0268	.01707	1.57	1660	.06112	.01069	5.718	1039
15.5	.03296	.02197	1.5	2135	.07944	.01446	5.494	1406
18.5	.03752	.02558	1.467	2485	.0904	.0167	5.413	1624
21.5	.0426	.0314	1.357	3050	.1048	.0201	5.214	1954

5-inch circular cylinder p_o = 12 psia

X, in	δ^*_{inc}, in	θ_{inc}, in	H_{inc}	R_{θ} inc	δ^*_{comp}, in	θ_{comp}, in	H_{comp}	R_{θ} comp
.5	.00974	.00307	3.173	512	.01414	.00146	9.685	243.7
3.5	.02154	.00642	3.355	1072	.03046	.0032	9.519	534
6.5								
9.5	.01872	.01204	1.555	2010	.04688	.0088	5.327	1469
12.5	.02608	.01384	1.384	3144	.06504	.01152	5.646	1923
15.5	.03232	.02236	1.445	3730	.08048	.01424	5.652	2375
18.5	.0376	.0266	1.414	4440	.0896	.0167	5.365	2788
21.5	.0458	.0315	1.454	5255	.11	.0205	5.366	3420

TABLE II continued

5-inch circular cylinder p_o = 20 psia

X, in	δ^*_{inc}, in	θ_{inc}, in	H_{inc}	R_{θ} inc	δ^*_{comp}, in	θ_{comp}, in	H_{comp}	R_{θ} comp
.5	.0085	.00266	3.196	748	.01246	.00116	10.741	326.2
3.5	.01604	.00507	3.164	1427	.02356	.00226	10.425	635.5
6.5	.01256	.00736	1.707	2070	.0284	.00452	6.283	1272
9.5	.0192	.01228	1.564	3454	.04608	.00828	5.565	2330
12.5	.02416	.01668	1.448	4690	.05944	.01076	5.524	3027
15.5	.02896	.02108	1.374	5925	.0748	.01348	5.55	3791
18.5	.034	.025	1.36	7030	.0864	.0161	5.367	4527
21.5	.0414	.0289	1.433	8125	.1004	.0193	5.202	5425

5-inch circular cylinder p_o = 30 psia

X, in	δ^*_{inc}, in	θ_{inc}, in	H_{inc}	R_{θ} inc	δ^*_{comp}, in	θ_{comp}, in	H_{comp}	R_{θ} comp
.5	.00844	.00262	3.221	1113	.01248	.00119	10.487	505
3.5	.01244	.0047	2.647	1996	.01964	.00236	8.322	1003
6.5	.01336	.00884	1.511	3754	.0312	.00536	5.821	2277
9.5								
12.5	.02624	.01584	1.657	6720	.05832	.00896	6.509	3805
15.5	.02856	.02088	1.368	8860	.07224	.01264	5.715	5365
18.5	.0304	.0237	1.283	10070	.0826	.0152	5.434	6450
21.5	.0396	.0298	1.329	12660	.0996	.0192	5.19	8150

TABLE II continued

5-inch circular cylinder p_o = 50 psia

X, in	δ^*_{inc}, in	θ_{inc}, in	H_{inc}	R_{θ} inc	δ^*_{comp}, in	θ_{comp}, in	H_{comp}	R_{θ} comp
.5	.00846	.00331	2.556	2337	.01354	.00162	8.36	1144
3.5	.0114	.00578	1.972	4080	.02308	.00338	6.828	2387
6.5	.01648	.00992	1.661	7000	.038	.00608	6.25	4290
9.5	.02036	.01364	1.493	9620	.05024	.0084	5.98	5930
12.5	.024	.016	1.5	11300	.06	.01028	5.837	7250
15.5	.02608	.01916	1.361	13530	.06864	.0124	5.536	8750
18.5	.0292	.02064	1.415	14580	.07736	.01284	6.025	9060
21.5	.0336	.02528	1.329	17850	.0868	.01588	5.466	11210

Values of Boundary-Layer Parameters for Data of Reference f, M = 2.41
Stream Turbulence unknown

1.87-inch circular cylinder p_o = 7 inches Hq abs

X, in	δ^*_{inc}, in	θ_{inc}, in	H_{inc}	θ_{comp}, in	R_{θ} inc	R_{θ} comp
0.58	.00904	.00384	2.354	.0023	234	140
1.58	.0160	.00536	2.985	.0034	315	200
2.58	.01996	.0062	3.2194	.0042	369	250
3.58	.01988	.00856	2.3224	.00525	506	310
4.58	.02616	.00916	2.8559	.0057	562	350
5.58	.02936	.01156	2.539	.00700	694	420
6.58	.02288	.00972	2.354	.00605	594	370
8.08	.03564	.01124	3.171	.0073	693	450

TABLE II continued

1.87-inch circular cylinder p_o = 30 inches Hq abs

X, in	δ^*_{inc}, in	θ_{inc}, in	H_{inc}	θ_{comp}, in	R_θ inc	R_θ comp
0.58	.00592	.00272	2.177	.0014	680	350
1.58	.00792	.00356	2.225	.00195	912	500
2.58	.00900	.00368	2.935	.00215	924	540
3.58	.01108	.00428	2.589	.0026	1055	640
4.58	.01168	.00484	2.413	.0028	1210	700
5.58	.01224	.00556	2.201	.0031	1365	760
6.58	.00972	.00516	1.884	.0031	1282	770
8.08	.00724	.00552	1.312	.0041	1440	1070

1.87-inch circular cylinder p_o = 60 inches Hq abs

X, in	δ^*_{inc}, in	θ_{inc}, in	H_{inc}	θ_{comp}, in	R_θ inc	R_θ comp
0.58	.00424	.00248	1.7097	.0012	1260	610
1.58	.00656	.00264	2.485	.0016	1305	790
2.58	.00724	.00292	2.48	.00175	1435	860
3.58	.00760	.00356	2.135	.0018	1740	880
4.58	.00616	.00352	1.750	.0019	1742	940
5.58	.0060	.00324	1.852	.0031	1620	1550
6.58	.0076	.00612	1.242	.0043	3770	2650
8.08	.01088	.00768	1.417	.0059	3970	3050

TABLE II concluded

1.87-inch circular cylinder p_o = 90 inches Hq abs

X, in	δ^*_{inc}, in	θ_{inc}, in	H_{inc}	θ_{comp}, in	R_θ inc	R_θ comp
0.58	.00256	.00204	1.255	.0012	1515	890
1.58	.00304	.00228	1.333	.00165	1657	1200
2.58	.00492	.00376	1.3085	.0025	2780	1850
3.58	.00444	.0034	1.306	.0022	2426	1570
4.58	.00632	.0038	1.663	.0031	2660	2170
5.58	.00736	.00508	1.449	.0042	3630	3000
6.58	.00964	.00736	1.310	.0053	5280	3800
8.08	.01160	.0092	1.261	.00665	6640	4800

1.87-inch circular cylinder p_o = 120 inches Hq abs

X, in	δ^*_{inc}, in	θ_{inc}, in	H_{inc}	θ_{comp}, in	R_θ inc	R_θ comp
0.58	.00212	.00144	1.472	.0011	1360	1040
1.58	.00380	.00264	1.44	.0018	2464	1630
2.58	.00532	.00380	1.40	.0028	3600	2650
3.58	.00568	.00376	1.511	.0028	3560	2650
4.58	.00672	.00508	1.323	.0038	4810	3600
5.58	.00912	.00636	1.434	.0047	5680	4200
6.58				.0057		5800
8.08	.01212	.00968	1.252	.0070	9260	6700

TABLE III

Values of Boundary-Layer Parameters for Data of Reference h
Stream turbulence 0.3 percent
NACA 0009 airfoil

$C_l = -0.57$

$\frac{s}{c}$	δ^*, in	θ, in	H	R_θ	$R_\theta \frac{\theta}{u_\infty} \frac{du_\infty}{dx}$
.05	.011125	.00465	2.392	211.2	.0294
.10	.01409	.00655	2.151	297.5	.0262
.20	.02057	.00984	2.09	446.8	.0188
.30	.02669	.01238	2.16	561.5	.0156
.35	.0308	.01487	2.07	675	.0181
.45	.03292	.01818	1.812	816.5	.0176
.55	.03266	.02024	1.623	850	.00981

$C_l = 0$

$\frac{s}{c}$	δ^*, in	θ, in	H	R_θ	$R_\theta \frac{\theta}{u_\infty} \frac{du_\infty}{dx}$
.06	.0157	.00538	2.918	244.2	- .00874
.11	.02	.007575	2.64	344	- .0165
.21	.0296	.01281	2.31	581.5	- .0417
.31	.03109	.01605	1.937	714	- .0553
.36	.0262	.0167	1.569	705	- .0473
.46	.0267	.0171	1.561	691	- .0376
.56	.0256	.01725	1.484	638	- .0266

$C_l = 0.65$

$\frac{s}{c}$	δ^*, in	θ, in	H	R_θ
.07	.0248	.0154	1.610	699
.12	.0323	.0202	1.599	839
.22	.0274	.0181	1.514	641
.32	.02549	.01686	1.512	559
.47	.0242	.0164	1.476	510
.57	.021	.0132	1.591	381
.67	.021	.014	1.5	413.2

TABLE III continued

NACA 0012 airfoil

$C_l = -0.57$

$\frac{s}{c}$	δ^*, in	θ, in	H	R_θ	$R_\theta \frac{\theta}{u_\infty} \frac{du_\infty}{dx}$
.05	.01014	.003892	2.603	176.8	- .0396
.15	.01805	.007695	2.346	349.5	- .0245
.25	.02522	.01027	2.456	466.5	- .0156
.35	.026	.0125	2.08	568	- .00763
.45	.0236	.0128	1.844	564	+ .00188
.55	.03138	.0164	1.913	704	+ .00693
.70	.03116	.01873	1.663	756	+ .0292

$C_l = 0$

$\frac{s}{c}$	δ^*, in	θ, in	H	R_θ	$R_\theta \frac{\theta}{u_\infty} \frac{du_\infty}{dx}$
.07	.0118	.0049	2.408	222.6	- .00949
.17	.0224	.00886	2.528	402.5	.0207
.27	.0287	.0109	2.633	495	.0300
.37	.0275	.0164	1.677	726	.0708
.47	.0235	.0162	1.451	677	.0598
.57	.0234	.01535	1.525	578.5	.0448
.72	.02177	.0157	1.386	534.5	.0384

$C_l = 0.65$

$\frac{s}{c}$	δ^*, in	θ, in	H	R_θ
.18	.02697	.01693	1.593	722.5
.28	.0284	.01852	1.533	693.5
.38	.02408	.0158	1.524	538
.48	.0232	.01661	1.397	539.5
.58	.02169	.01445	1.502	436.3
.73	.02298	.01452	1.582	412

TABLE III concluded

NACA 0018 airfoil

$C_l = -0.57$

$\frac{s}{c}$	δ^*, in	θ, in	H	R_θ	$R_\theta \frac{\theta}{u_\infty} \frac{du_\infty}{dx}$
.06	.0092	.00438	2.1	198.9	.0293
.16	.0164	.0073	2.246	331.4	.0223
.26	.02097	.00948	2.212	430.3	- .00328
.36	.0272	.01088	2.5	494	
.46	.03304	.01656	1.996	729.5	- .0388
.56	.0277	.01589	1.744	674	- .0262
.66	.02252	.01474	1.528	575.5	- .00284

$C_l = 0$

$\frac{s}{c}$	δ^*, in	θ, in	H	R_θ	$R_\theta \frac{\theta}{u_\infty} \frac{du_\infty}{dx}$
.08	.013	.0055	2.363	249.7	.0203
.18	.02158	.00846	2.55	384.2	.0105
.28	.02656	.01136	2.336	516	- .148
.38	.0244	.01588	1.537	692	- .203
.48	.02204	.01444	1.527	557	- .115
.58	.0232	.01608	1.443	595	- .106
.68	.02292	.01504	1.525	525.5	- .0801

$C_l = 0.65$

$\frac{s}{c}$	δ^*, in	θ, in	H	R_θ	$R_\theta \frac{\theta}{u_\infty} \frac{du_\infty}{dx}$
.10	.0113	.00494	2.287	224.3	.0643
.20	.02128	.0133	1.6	604	1.534
.30	.02744	.018	1.525	736	- 1.676
.40	.0248	.0162	1.531	596	- .406
.50	.02356	.01476	1.595	489.4	- .172
.60	.02292	.01546	1.483	481	- .114
.70	.01968	.01268	1.553	363	- .0460

TABLE IV

Values of Boundary-Layer Parameters for Data of Reference 1
Stream Turbulence Unknown

U_o = 60 ft/sec

$\frac{s}{c}$	δ^*, in	θ, in	H	R_θ	$R_\theta \frac{\theta}{u_\infty} \frac{du_\infty}{dx}$
.0524	.00835	.004045	2.067	145.9	.0141
.1007	.1239	.00578	2.144	215	.00715
.151	.01578	.00759	2.08	286.8	
.202	.01998	.00934	2.139	354.5	
.252	.0216	.00978	2.209	371	- .00261
.302	.03081	.01655	1.862	628	- .0210
.403	.03073	.02025	1.518	743	- .0584
.504	.04137	.03033	1.364	1076	- .162
.605	.05717	.03994	1.431	1367	- .306
.706	.07971	.05645	1.412	1880	- .573
.807	.09655	.06888	1.402	2188	- .904
.956	.1424	.09917	1.436	2930	-1.428

U_o = 80 ft/sec

$\frac{s}{c}$	δ^*, in	θ, in	H	R_θ	$R_\theta \frac{\theta}{u_\infty} \frac{du_\infty}{dx}$
.0524	.00732	.0036	2.035	171.8	.0148
.1007	.0[illegible]13	.00519	2.174	258.4	.00771
.151	.01366	.00638	2.139	320.2	
.202	.01693	.008734	1.938	440	
.252	.01836	.01085	1.692	553.5	- .00432
.302	.02533	.01783	1.421	897	- .0324
.403	.02890	.02132	1.356	1045	- .0866
.504	.04431	.03275	1.353	1564	- .254
.605	.06479	.04693	1.381	2161	- .568
.706	.06908	.05129	1.347	2235	- .619
.807	.09909	.07178	1.381	3023	-1.302
.956	.1404	.09655	1.454	3804	-1.805

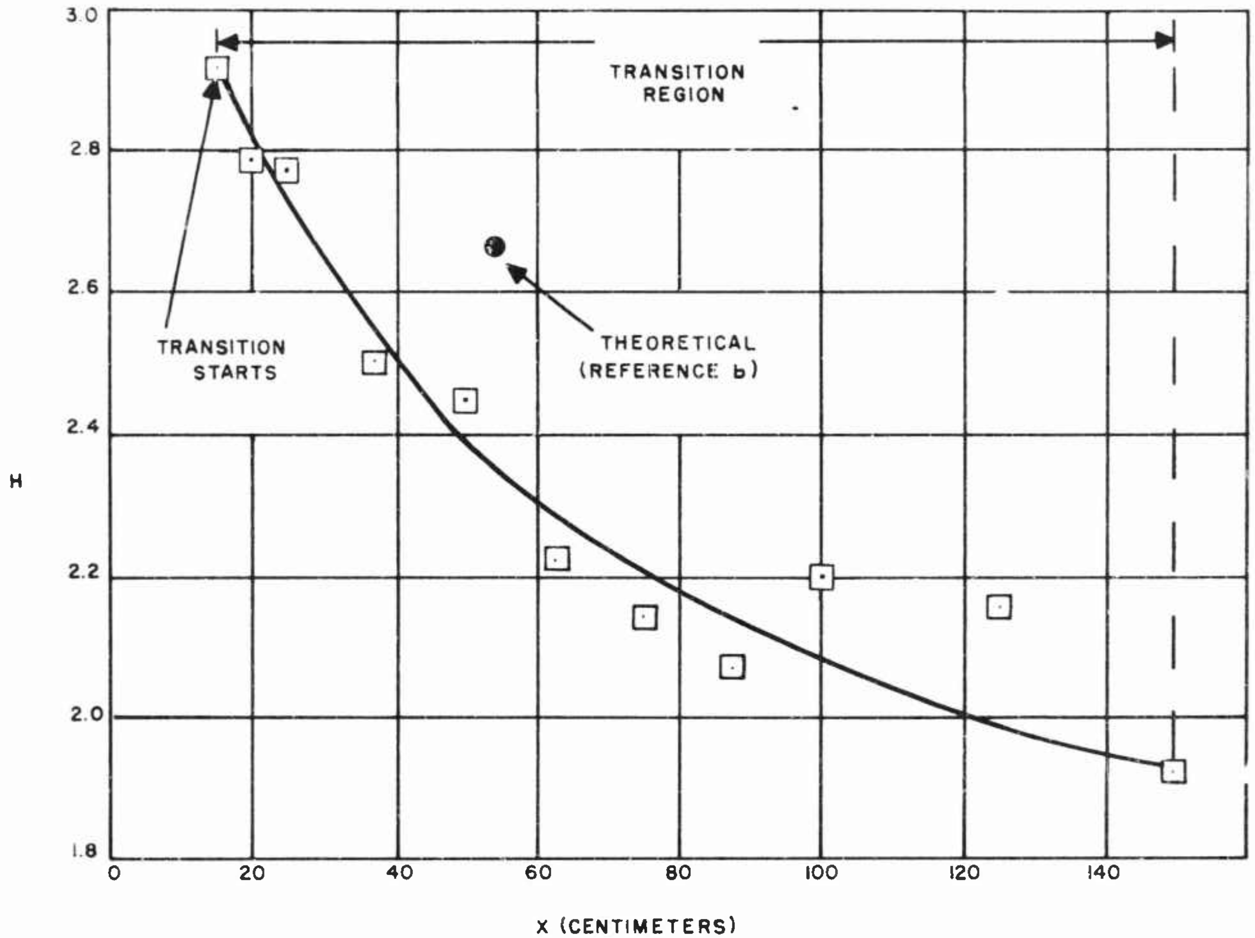

A. TUNNEL AIRSPEED: 400 CENTIMETERS PER SECOND

FIG. I VARIATION OF H WITH DISTANCE ALONG A FLAT PLATE (DATA OF REF. d)

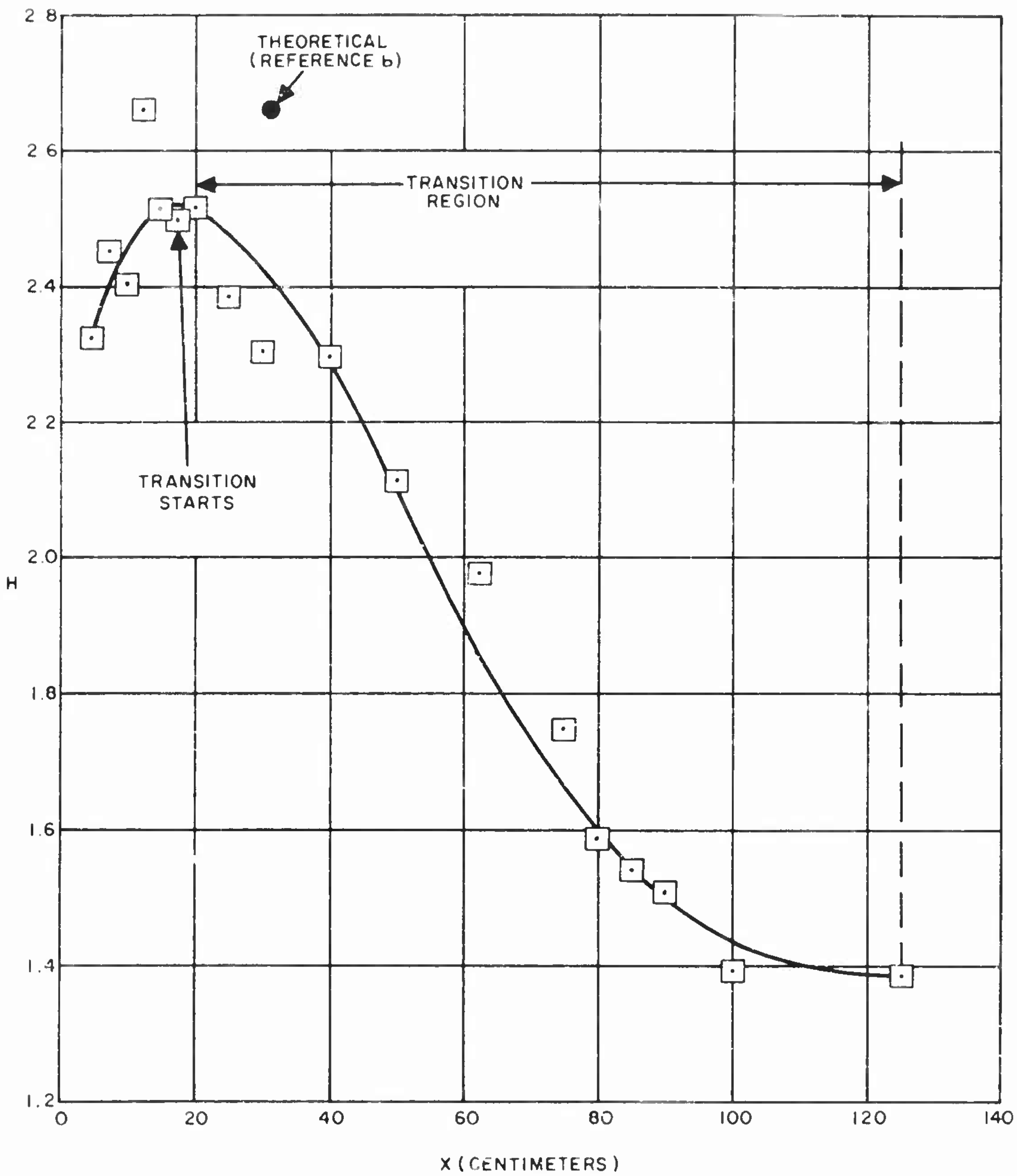

B. TUNNEL AIRSPEED: 800 CENTIMETERS PER SECOND

FIG. I CONTINUED

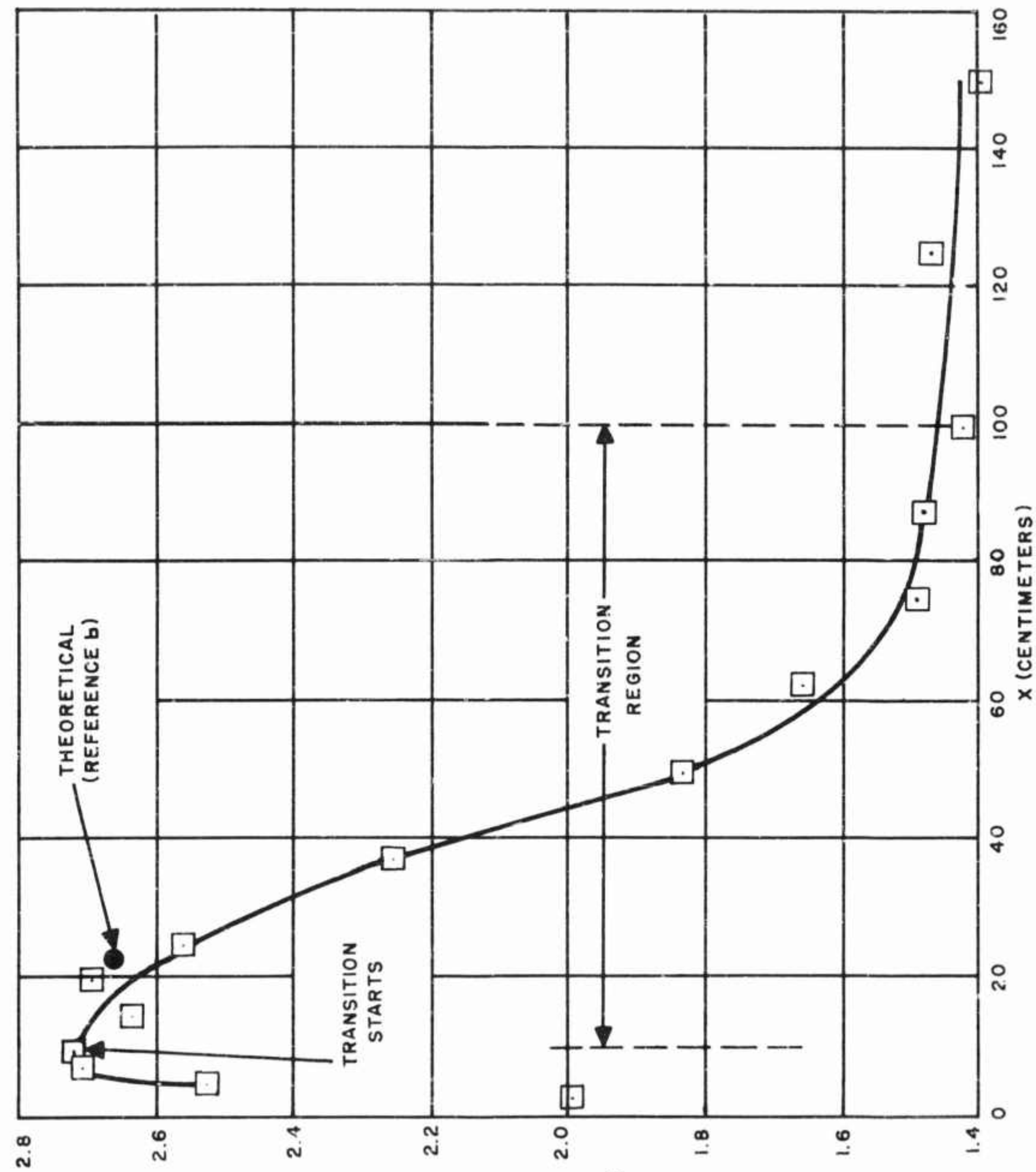

C. TUNNEL AIRSPEED: 1200 CENTIMETERS PER SECOND
FIG.1 CONTINUED

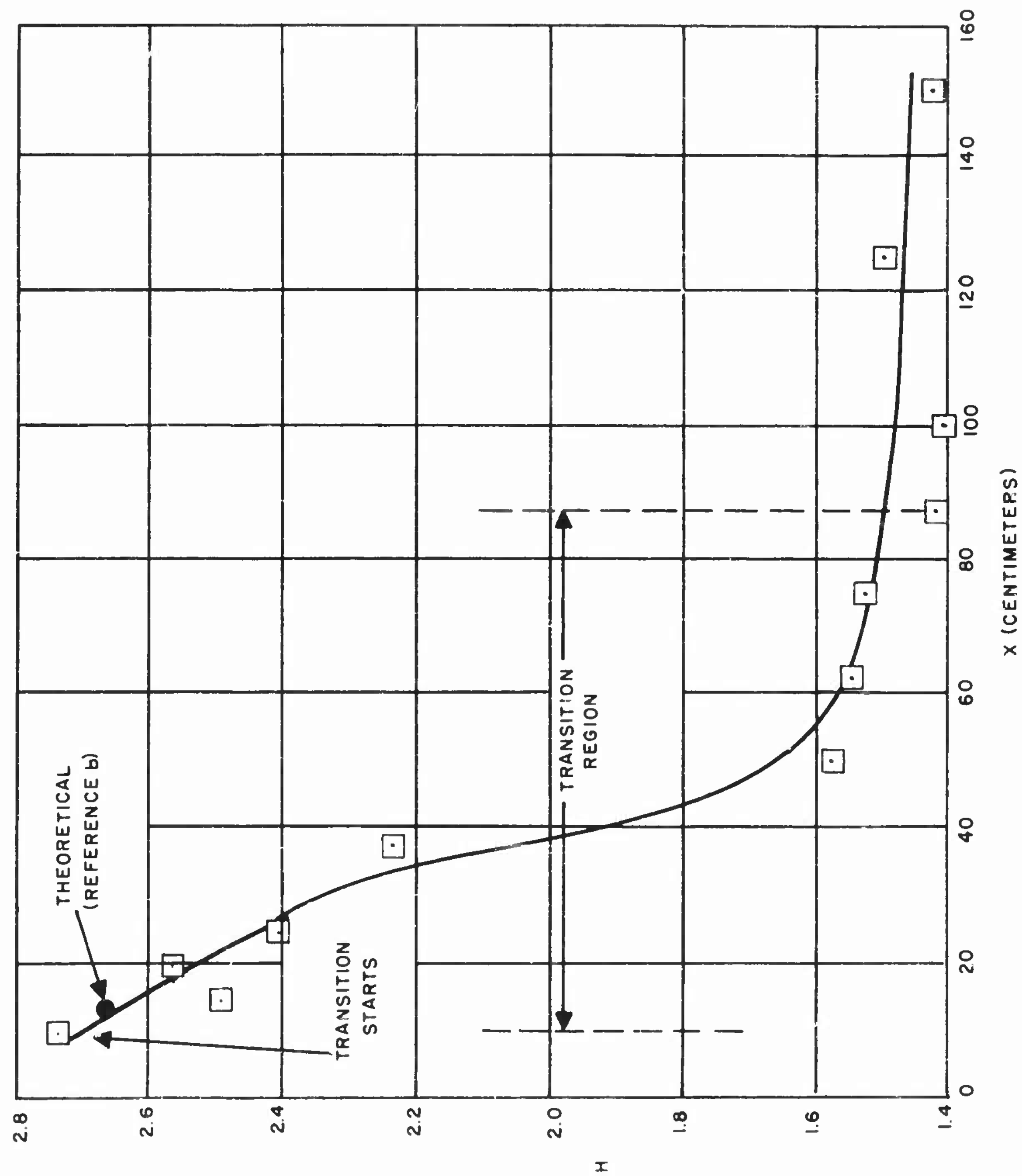

D. TUNNEL AIRSPEED: 1600 CENTIMETERS PER SECOND

FIG.1 CONTINUED

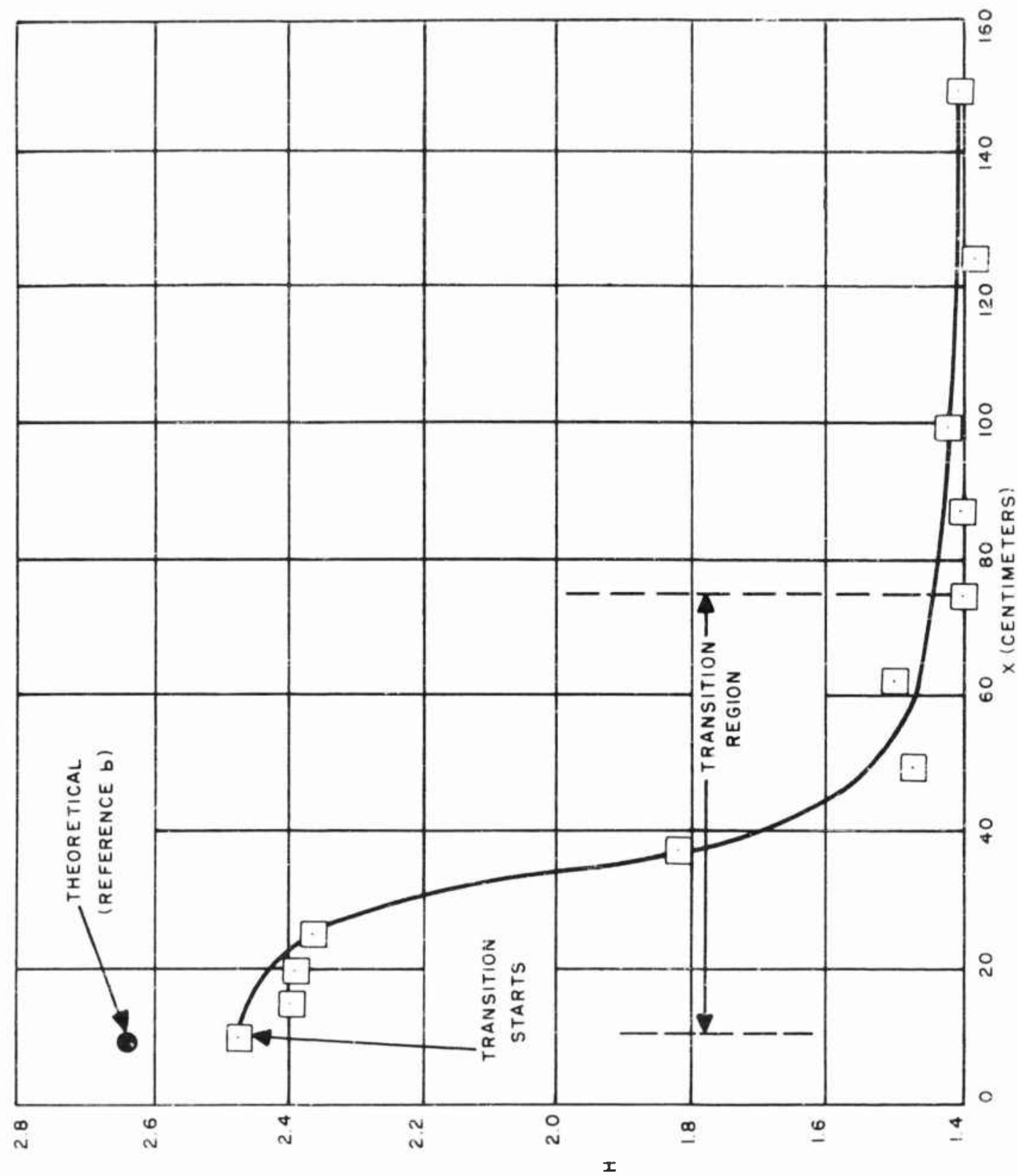

E. TUNNEL AIRSPEED: 2400 CENTIMETERS PER SECOND

FIG. I CONTINUED

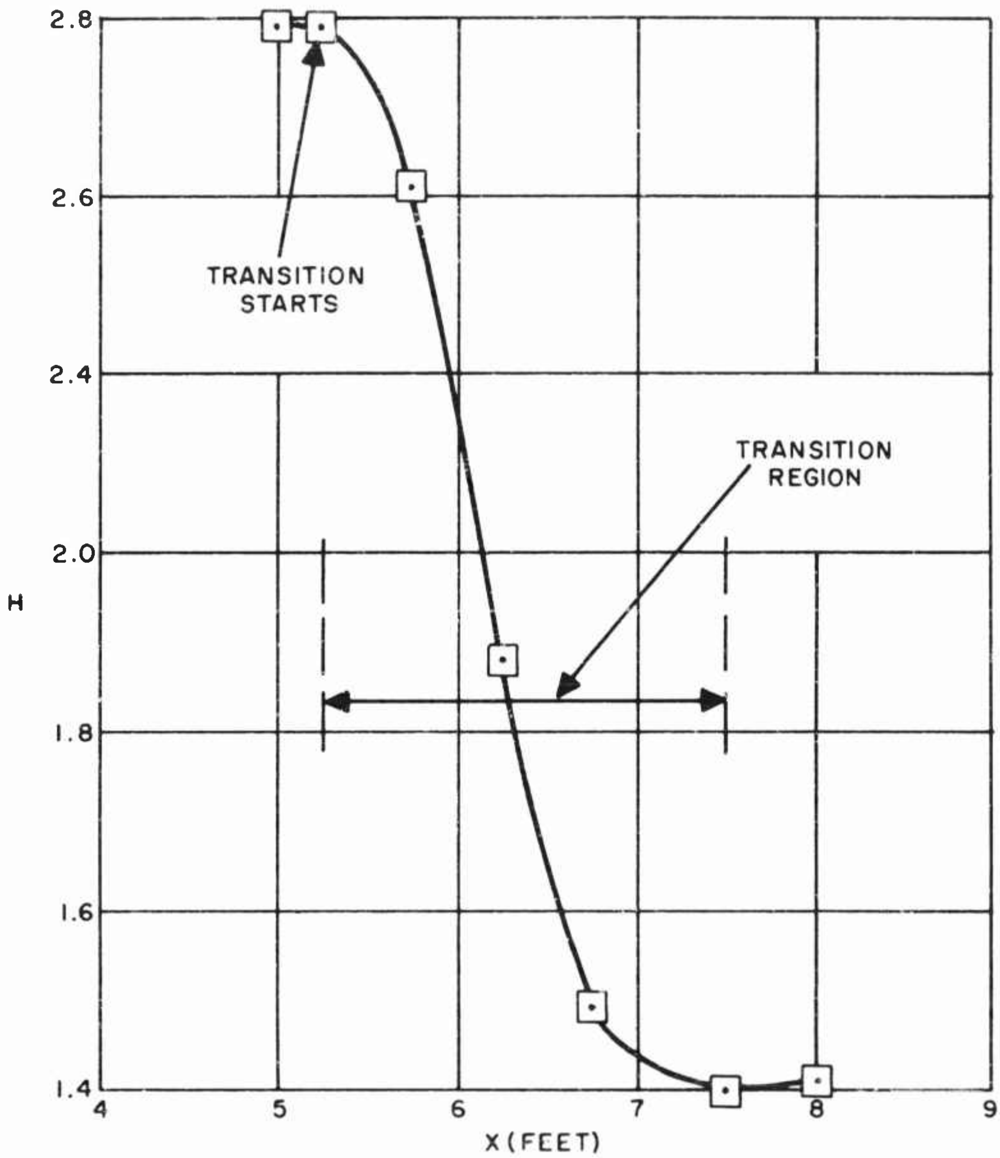

FIG. 2 VARIATION OF H WITH DISTANCE ALONG FLAT PLATE

(DATA OF REFERENCE e)

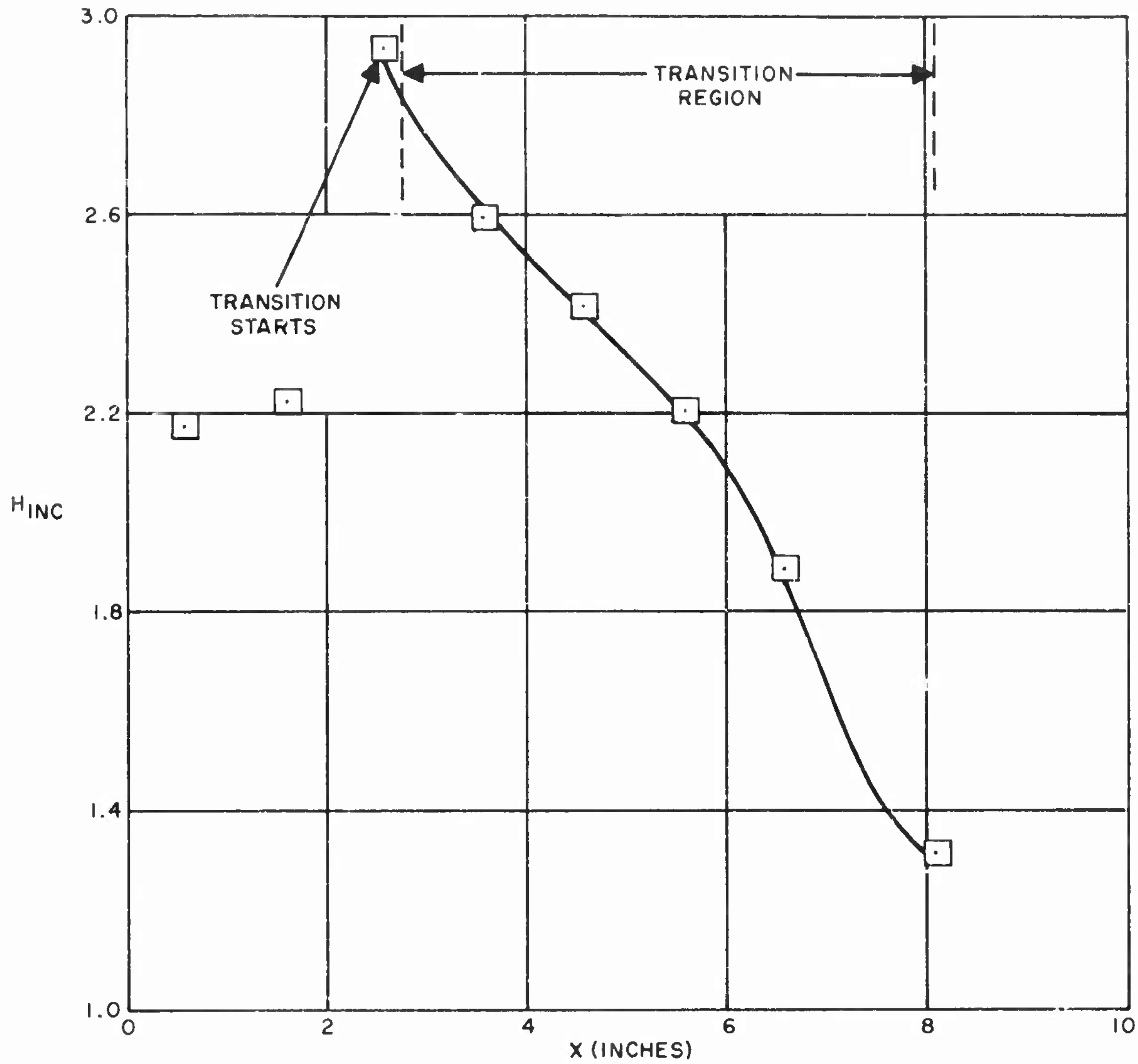

A. 1.87-INCH DIAMETER; P_0 = 30-INCH Hg ABSOLUTE

FIG.3 VARIATION OF H_{INC} WITH DISTANCE ALONG CIRCULAR CYLINDER IN AXIAL FLOW AT M=2.41 (DATA OF REFERENCE f)

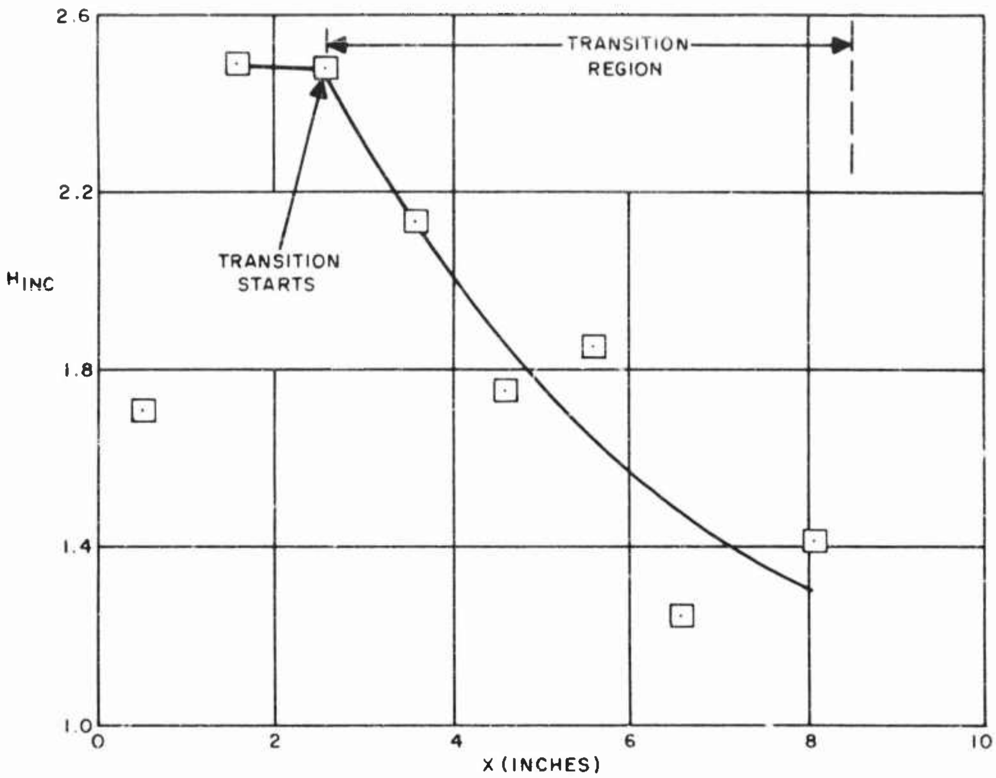

B. 1.87-INCH DIAMETER; P_0 = 60-INCH Hg ABSOLUTE

FIG. 3 CONCLUDED

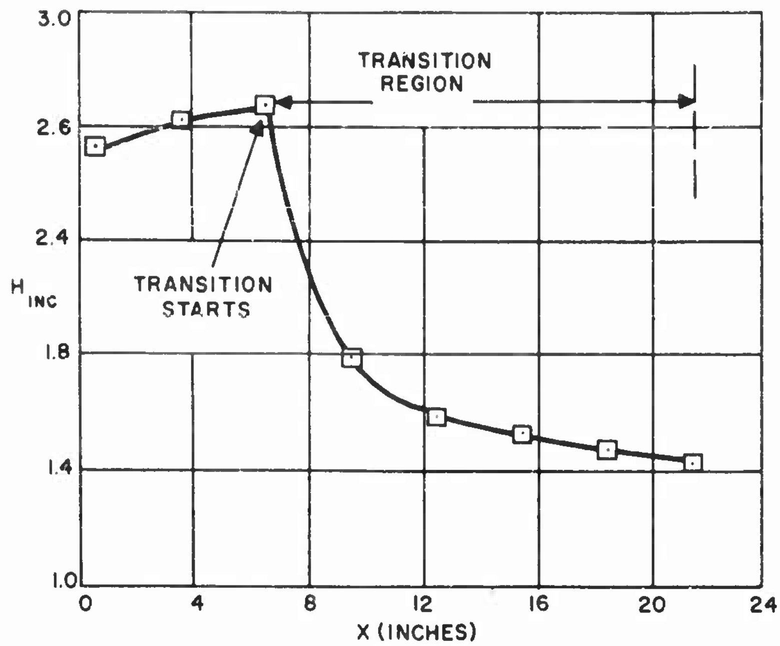

A. 3-INCH DIAMETER; Po = 12 PSIA

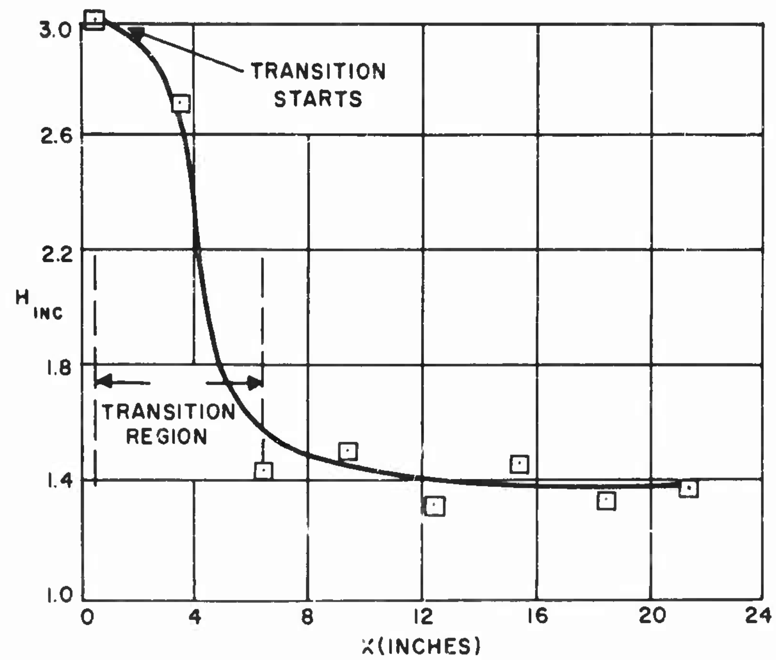

B. 3-INCH DIAMETER; Po = 50 PSIA

FIG. 4 VARIATION OF H_{INC} WITH DISTANCE ALONG CIRCULAR CYLINDER IN AXIAL FLOW AT M = 3.05 DATA OF REFERENCE g

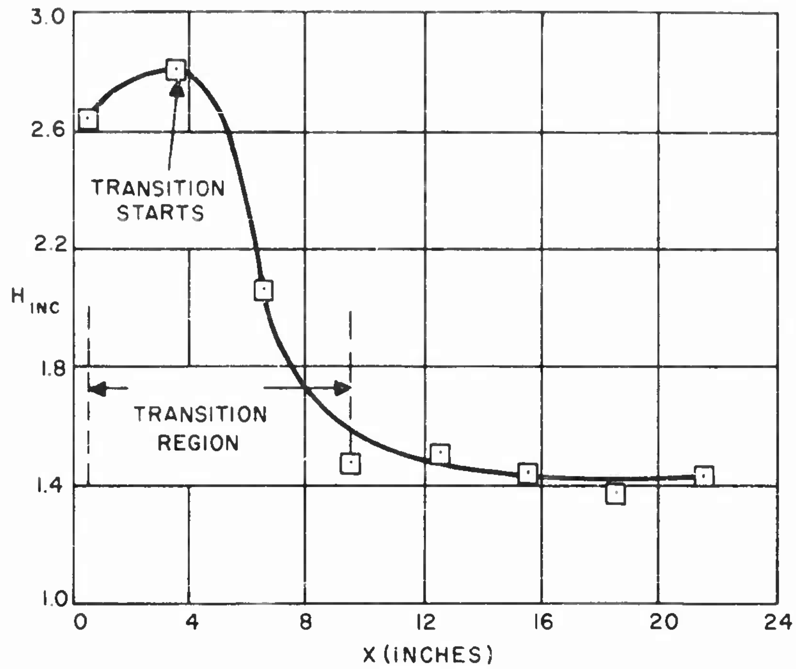

C. 4-INCH DIAMETER, Po=12 PSIA

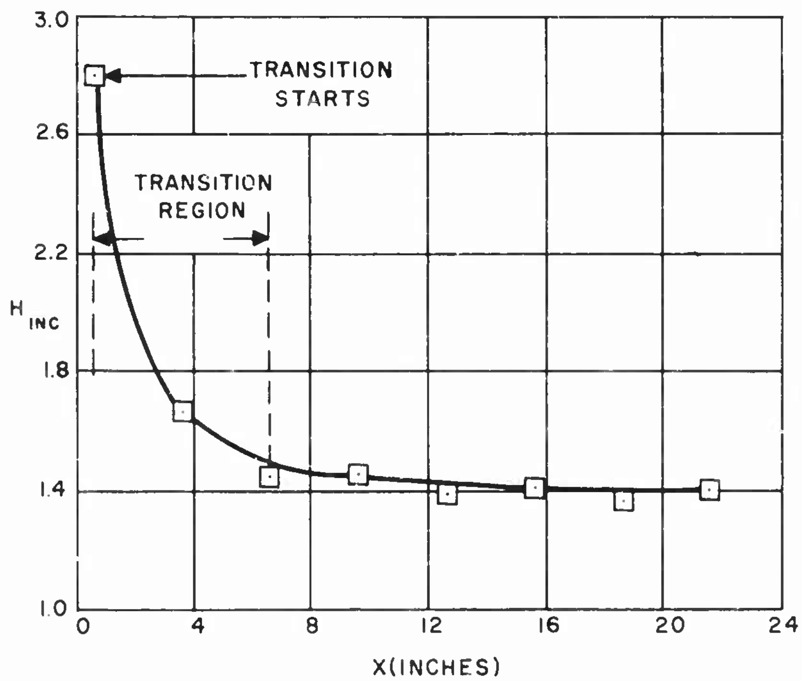

D. 4-INCH DIAMETER, Po=50 PSIA

FIG. 4 CONTINUED

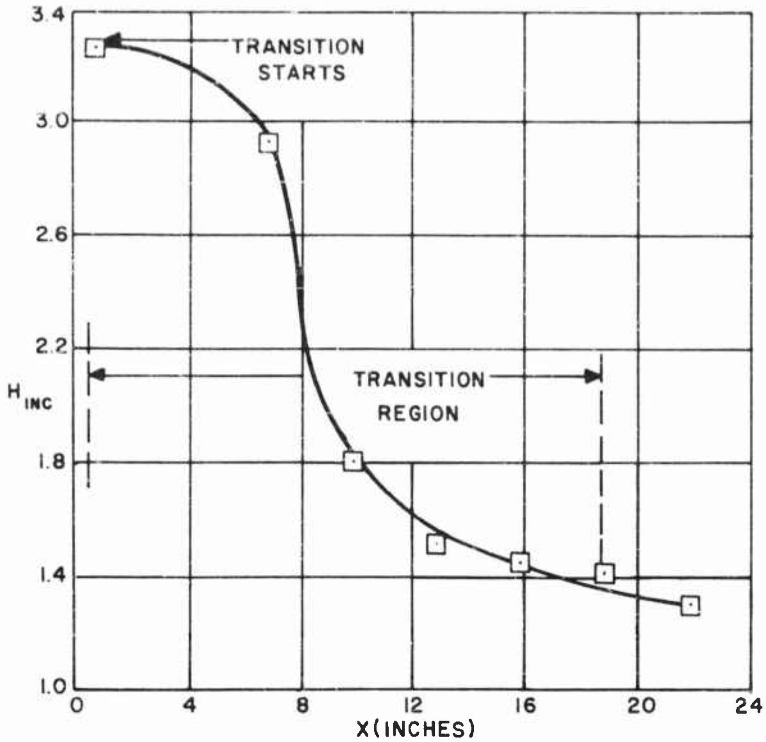

E. 5-INCH DIAMETER; Po=7 PSIA

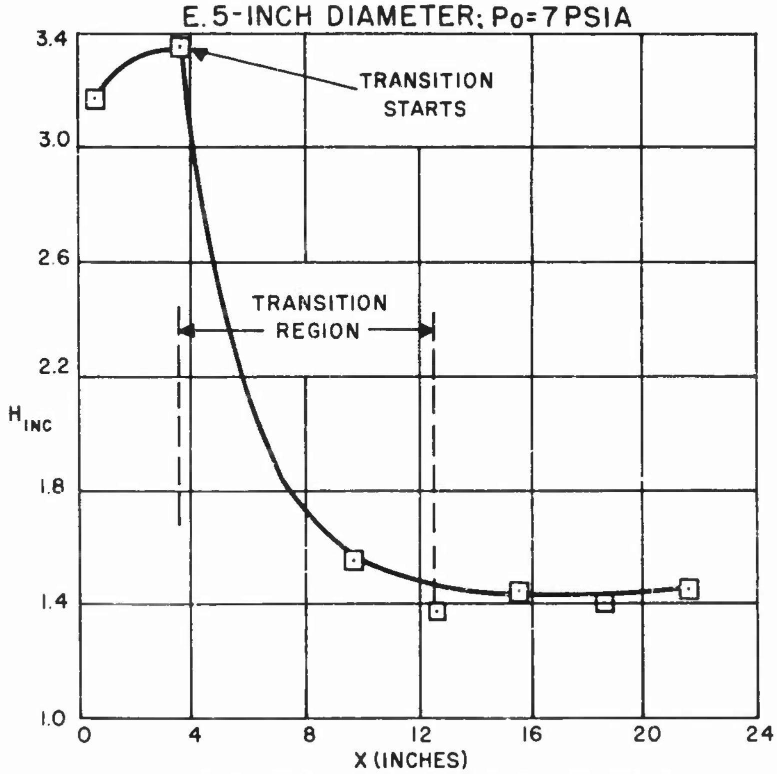

F. 5-INCH DIAMETER; Po = 12 PSIA

FIG. 4 CONTINUED

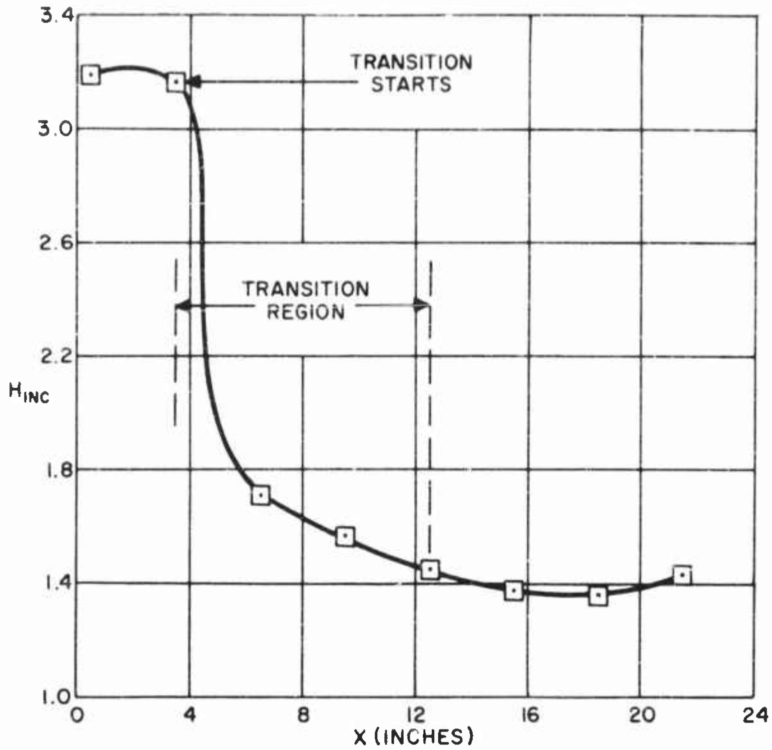

G. 5-INCH DIAMETER; P_0 = 20 PSIA

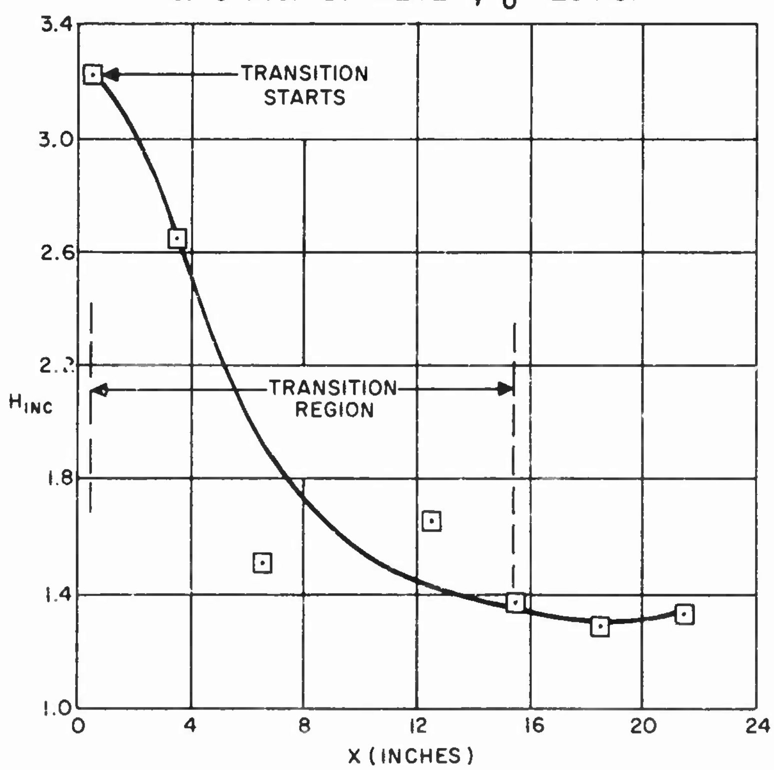

H. 5-INCH DIAMETER; P_0 = 30 PSIA

FIG. 4 CONTINUED

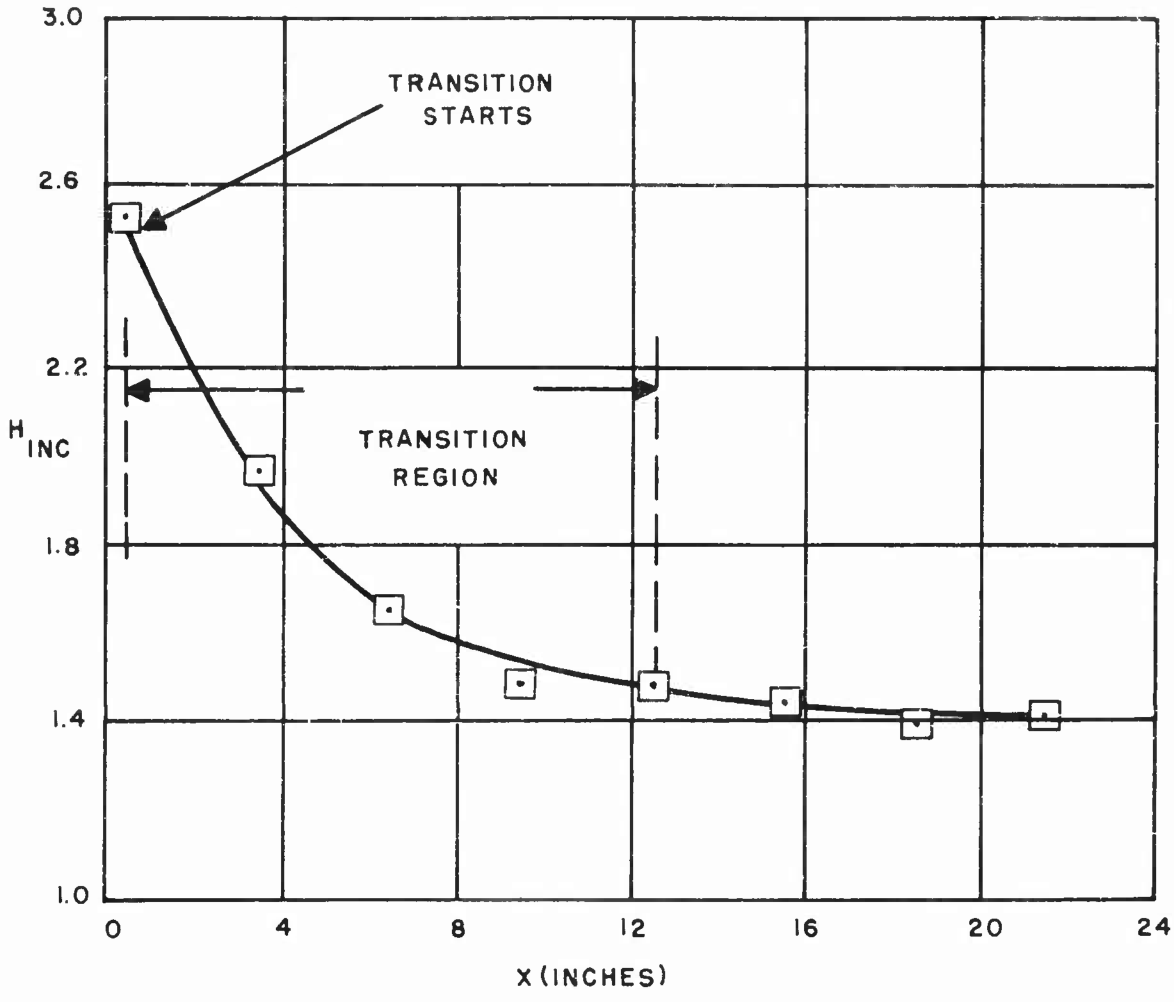

1. 5-INCH DIAMETER; Po = 50 PSIA

FIG. 4 CONCLUDED

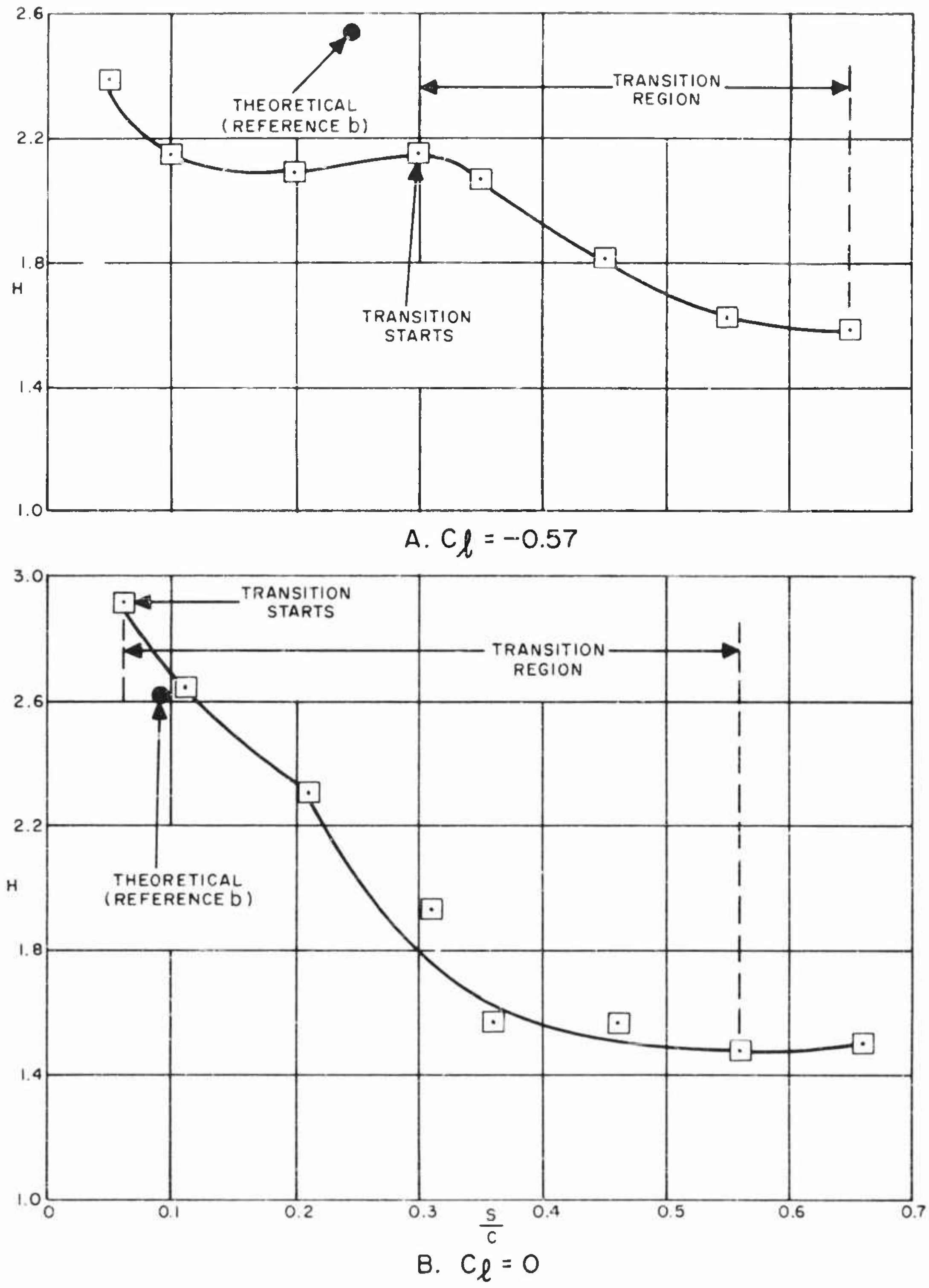

FIG. 5 VARIATION OF H WITH DISTANCE ALONG NACA 0009 AIRFOIL (DATA OF REFERENCE h)

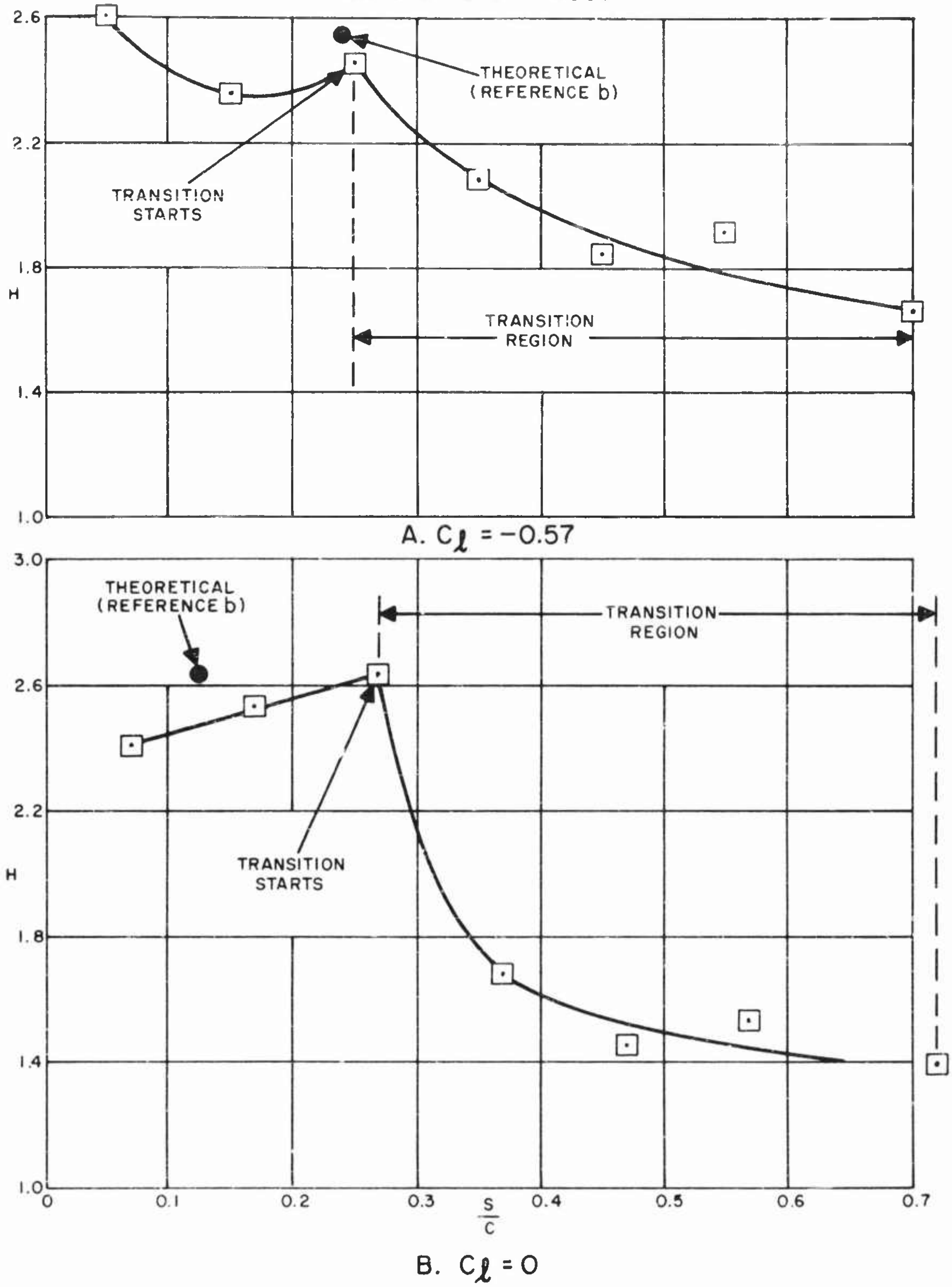

FIG. 6 VARIATION OF H WITH DISTANCE ALONG NACA 0012 AIRFOIL (DATA OF REFERENCE h)

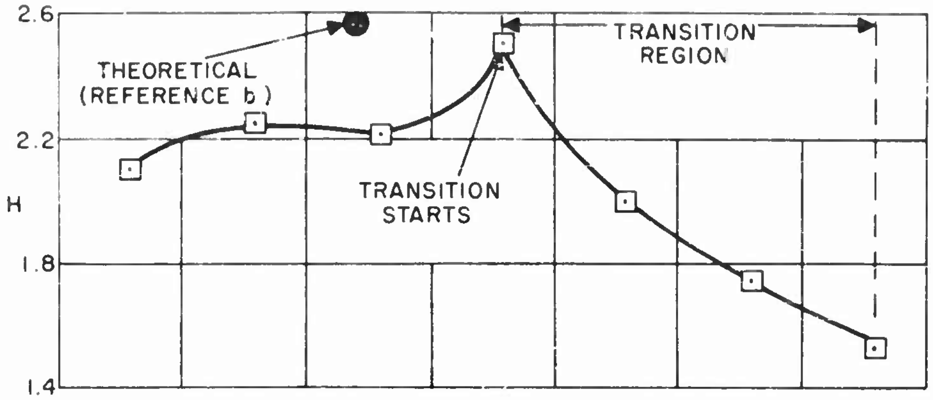

A. $C_\ell = 0.57$

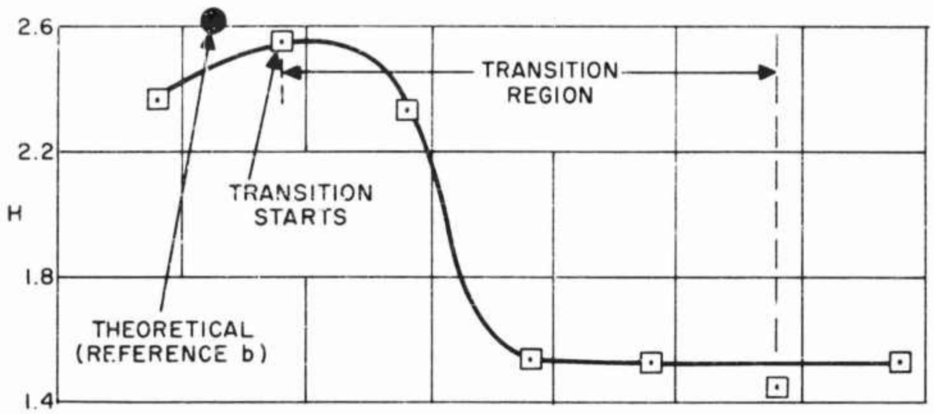

B. $C_\ell = 0$

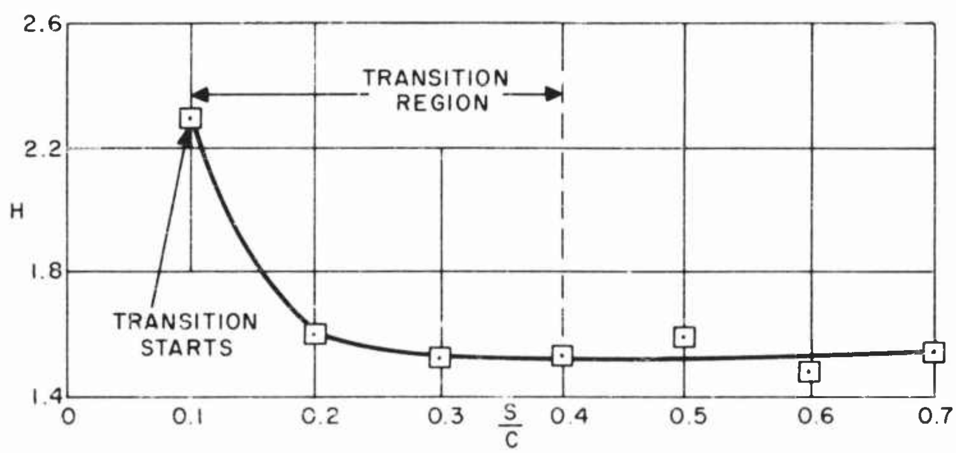

C. $C_\ell = 0.65$

FIG. 7 VARIATION OF H WITH DISTANCE ALONG NACA 0018 AIRFOIL (DATA OF REFERENCE h)

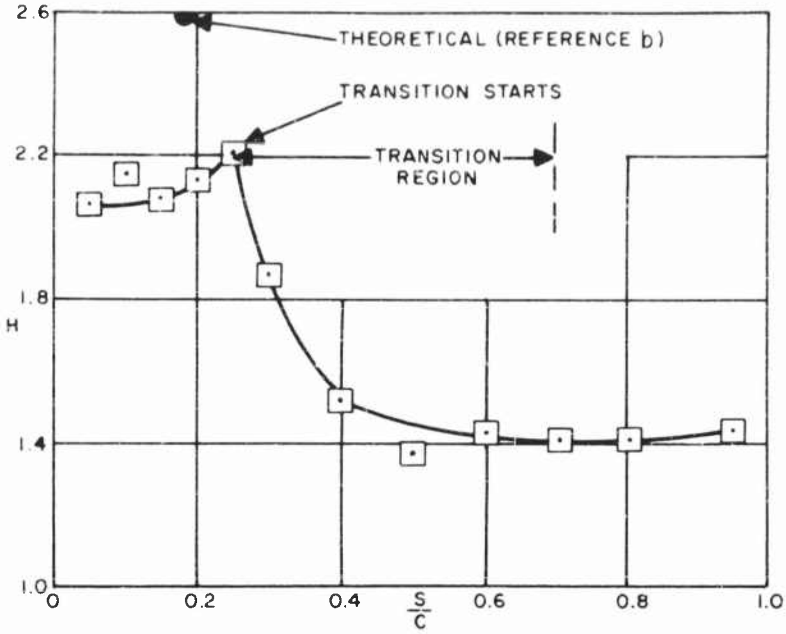

A. AIRSPEED: 60 FEET PER SECOND

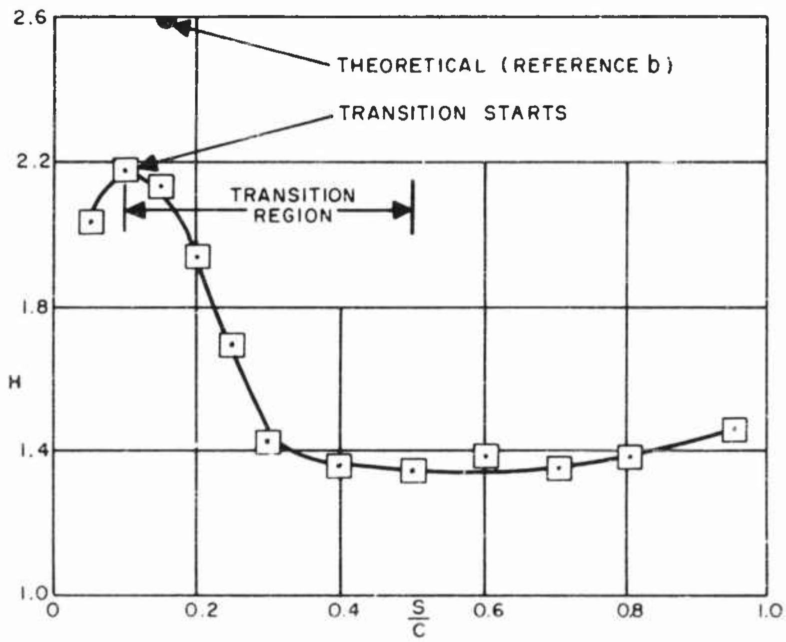

B. AIRSPEED: 80 FEET PER SECOND

FIG. 8 VARIATION OF H WITH DISTANCE ALONG SYMMETRICAL JOUKOWSKI AIRFOIL (DATA REFERENCE i)

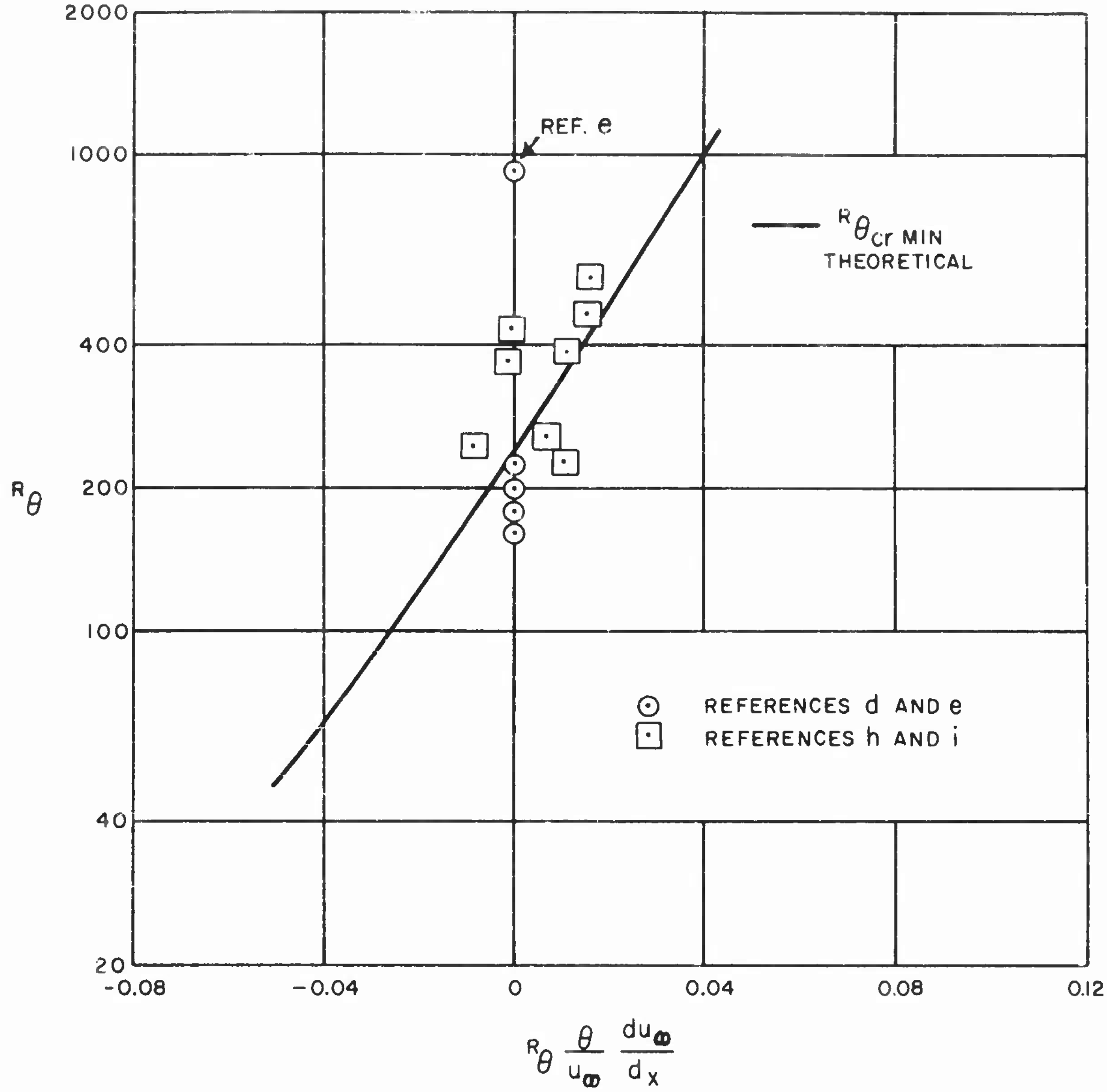

FIG. 9 COMPARISON BETWEEN THEORETICAL VALUES OF $R_{\theta_{cr\ MIN}}$ AND EXPERIMENTAL DATA AS A FUNCTION OF $R_\theta \frac{\theta}{u_\infty} \frac{du_\infty}{dx}$ FOR INCOMPRESSIBLE FLOW DATA

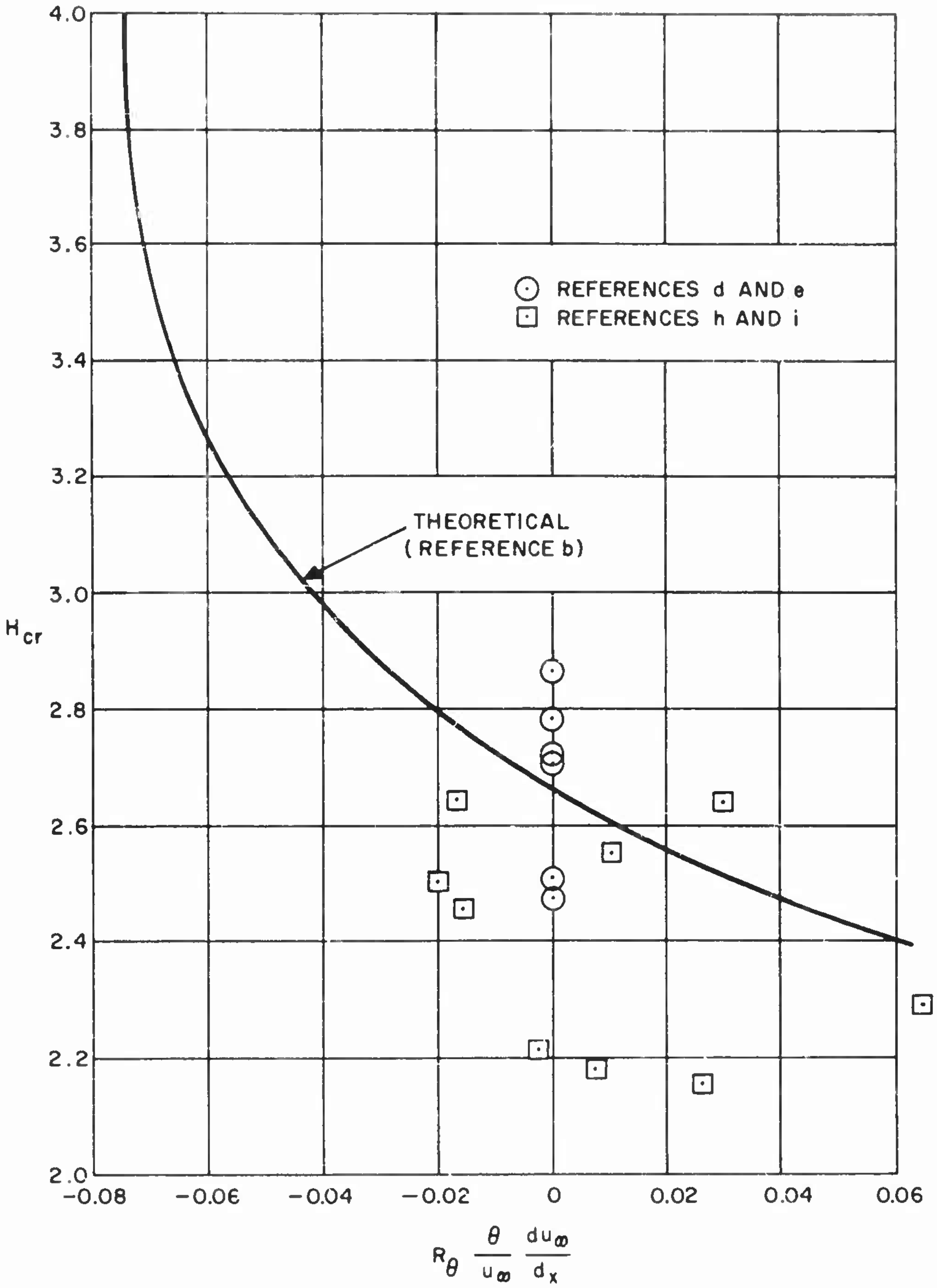

FIG. 10 COMPARISON BETWEEN THEORETICAL VALUES OF H_{cr} AND EXPERIMENTAL DATA AS A FUNCTION OF $R_\theta \frac{\theta}{u_\infty} \frac{du_\infty}{dx}$ FOR INCOMPRESSIBLE FLOW

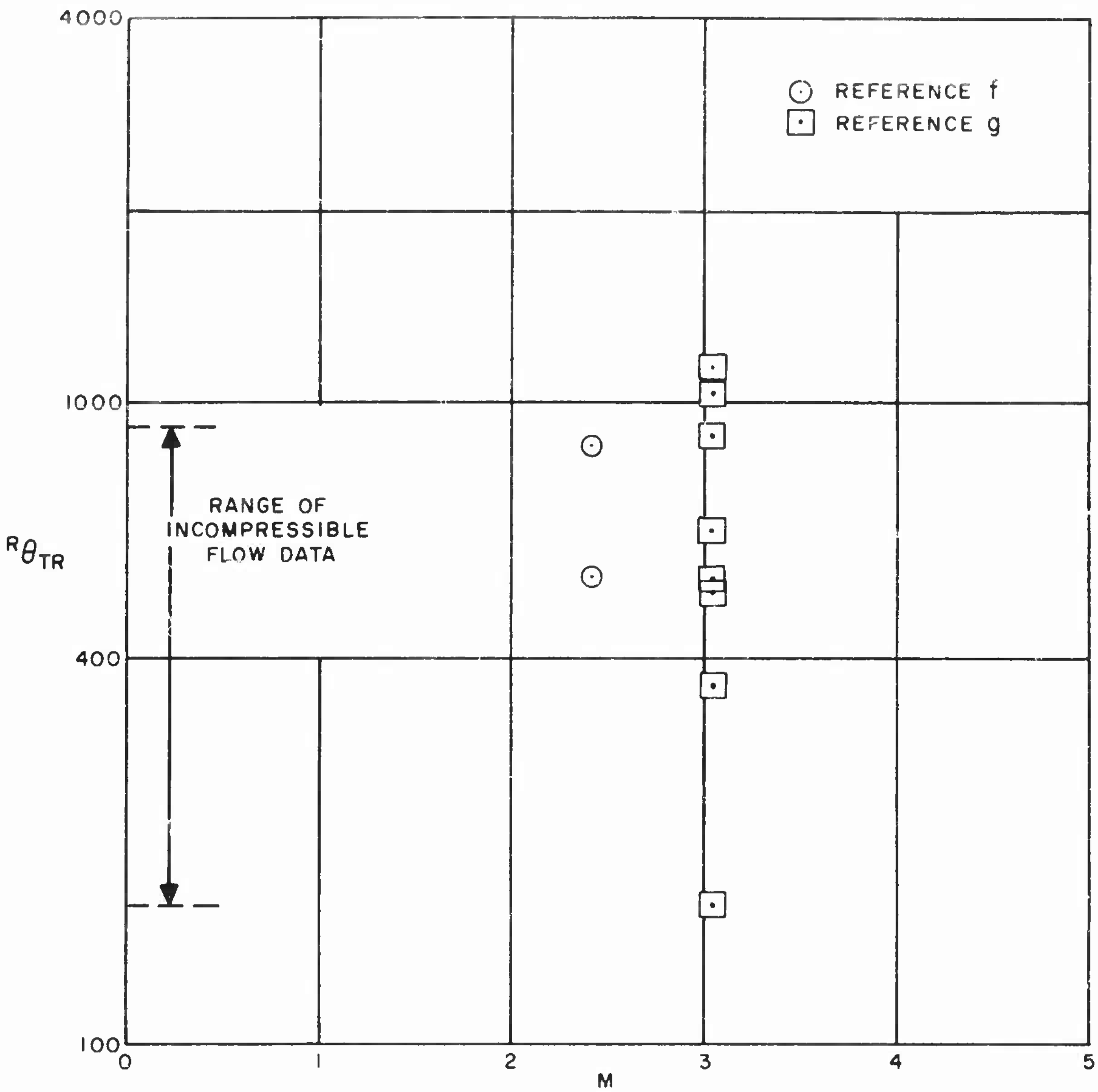

FIG. 11 VARIATION OF $R_{\theta_{TR}}$ WITH MACH NUMBER FOR COMPRESSIBLE FLOW DATA

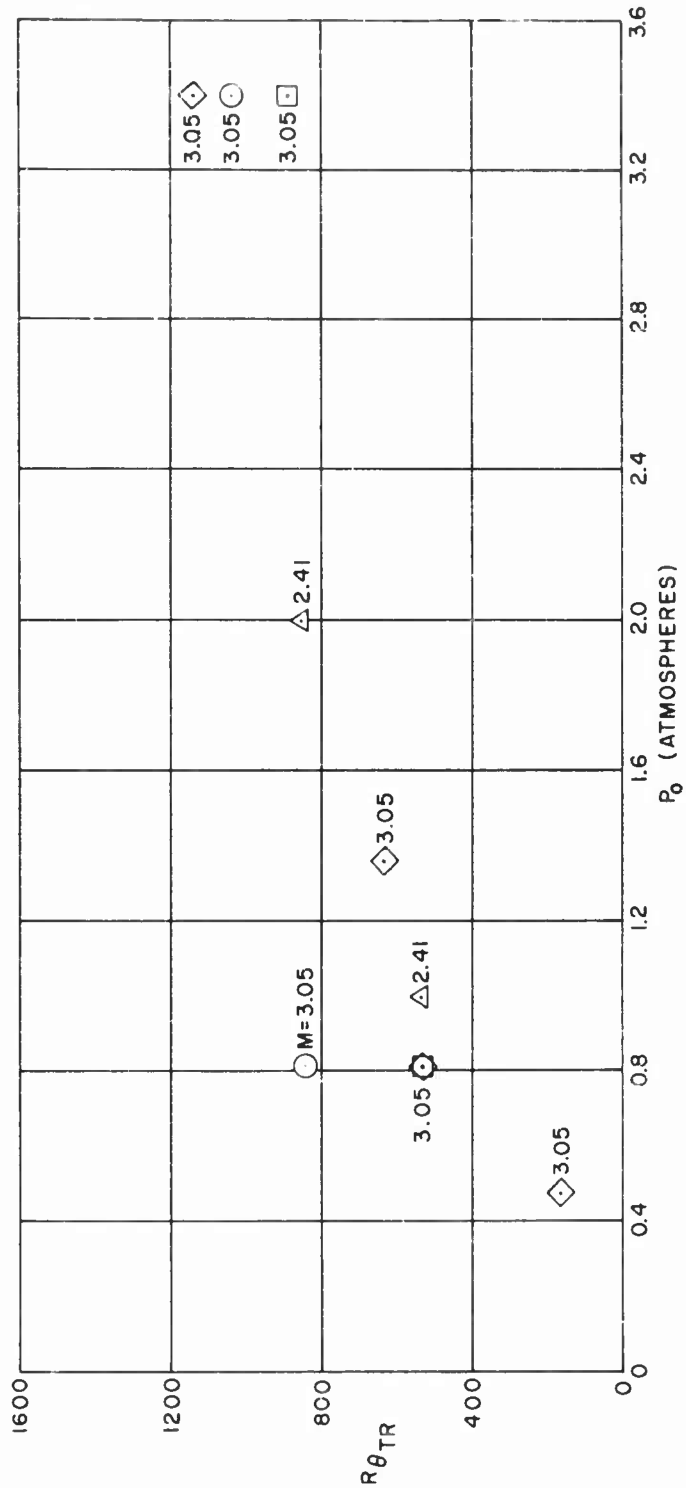

FIG.12 VARIATION OF $R_{\theta_{TR}}$ WITH SUPPLY PRESSURE FOR COMPRESSIBLE FLOW DATA

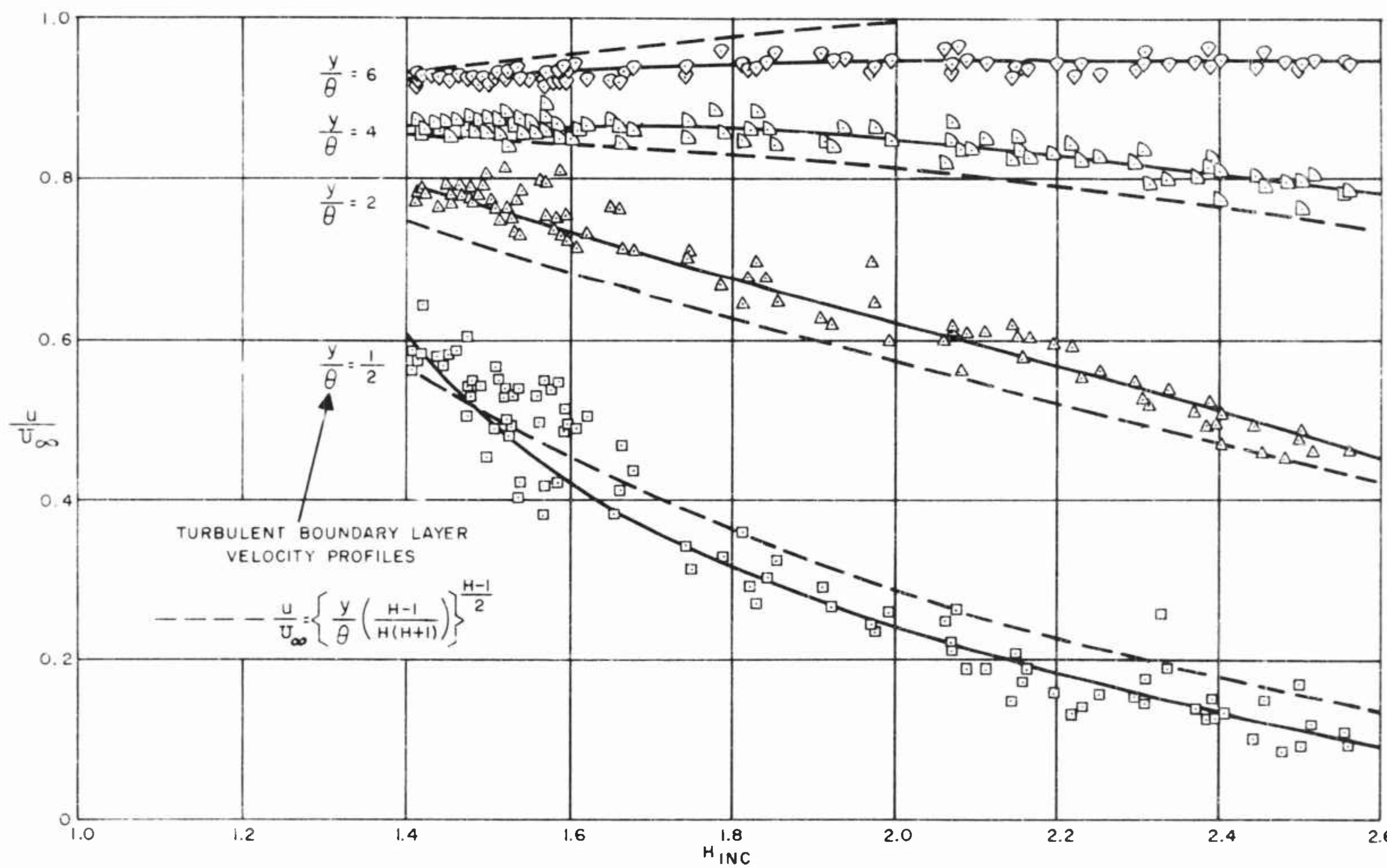

A. $\frac{y}{\theta} = \frac{1}{2}$, 2, 4, 6

FIG. 13 CORRELATION OF TRANSITION REGION VELOCITY PROFILE DATA

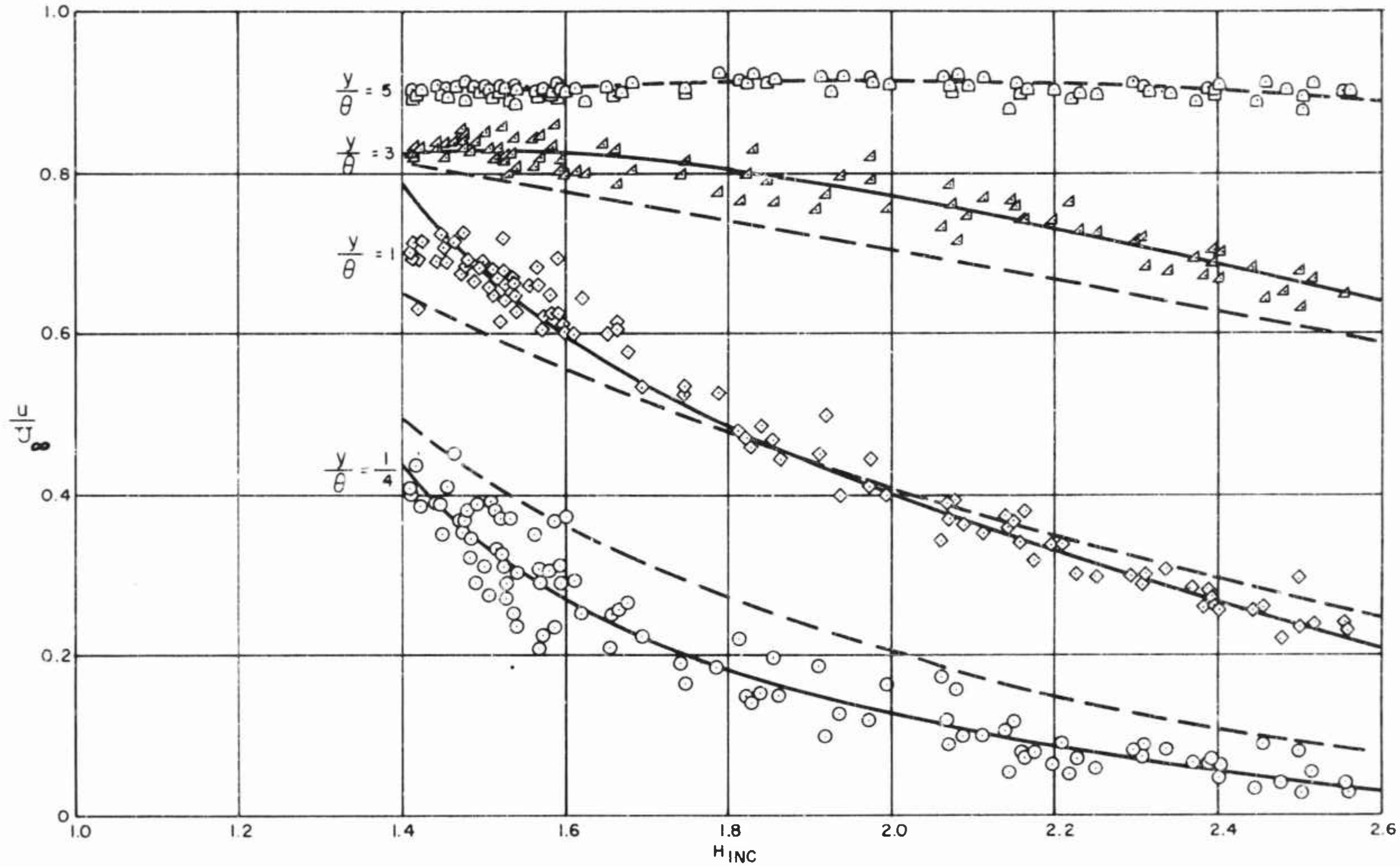

B. $\frac{y}{\theta} = \frac{1}{2}, 1, 3, 5$

FIG. 13 CONCLUDED

Aeroballistic Research Department
External Distribution List for Development (X1)

No. of Copies	
	Chief, Bureau of Ordnance Department of the Navy Washington 25, D. C.
1	Attn: Ad3
1	Attn: Ad6
1	Attn: Ree
1	Attn: Re3d
1	Attn: Re9a
	Chief, BuAer Washington 25, D. C.
3	Attn: TD-414
	Commander, U. S. NOTS Inyokern, China Lake, Calif.
1	Attn: Technical Library
1	Attn: Code 503
	Commander, NAMTC Point Mugu, California
2	Attn: Technical Library
	Superintendent U. S. Naval Postgraduate School Monterey, California
1	Attn: Tech. Rpts Section
	Director, NRL Washington 25, D. C.
1	Attn: Code 2021
	Officer in Charge, NPG Dahlgren, Virginia
1	Attn: Technical Library
	Office, Chief of Ordnance Department of the Army Washington 25, D. C.
1	Attn: ORDTU
	Office of the Assistant Secretary of Defense (R and D) Room 3 E 1065, The Pentagon Washington 25, D. C.
1	Attn: Technical Library
	Chief, AFSWP Washington 25, D. C.
1	Attn: Document Library Br.

No. of Copies	
	Commander, WADC Wright-Patterson AF Base Ohio
5	Attn: WCOSI-3
3	Attn: WCRRD
1	Attn: WCLGH-3
1	Director Air University Library Maxwell AF Base, Alabama
	Commanding General Aberdeen Proving Ground, Md.
1	Attn: Technical Info. Br.
1	Attn: Ballistics Res. Lab.
	Commanding General Redstone Arsenal Huntsville, Alabama
1	Attn: Aero. Lab, GMDD
5	ASTIA Document Service Center Knott Building Dayton 2, Ohio
	NACA High Speed Flight Station Box 273 Edwards Air Force Base, Calif.
1	Attn: Mr. W. C. Williams
	NACA Ames Aeronautical Laboratory Moffett Field, California
1	Attn: Librarian
	NACA Langley Aeronautical Lab. Langley Field, Virginia
1	Attn: Librarian
1	Attn: Mr. C. H. McLellan
1	Attn: Comp. Res. Div.
1	Attn: Adolf Busemann
1	Attn: John J. Stack
1	NACA Lewis Flight Propulsion Lab. 21000 Brookpark Road Cleveland 11, Ohio Attn: Librarian

No. of Copies	
1	NACA 1512 H Street, N. W. Washington 25, D. C.
	Commanding Officer, DOFL Washington 25, D. C.
1	Attn: Lib., Rm 211, Bldg 92
	Office of Naval Research Room 2709, T-3 Building Washington 25, D. C.
1	Attn: Head, Mechanics Br.
	Director of Intelligence Headquarters, USAF Washington 25, D. C.
1	Attn: AFOIN-3B
	Director, DTMB Aerodynamics Laboratory Washington 7, D. C.
1	Attn: Library
	University of California Berkeley 4, California
1	Attn: G. J. Maslach, 205-T3
2	Attn: Dr. S. A. Schaaf Via: ONR
	The University of Texas P. O. Box 8029 Austin 12, Texas
1	Attn: Defer se Res. Lab. Via: ONR
1	Applied Math. and Statistics Lab. Stanford University Stanford, California Via: ONR
	University of Michigan Willow Run Research Center Willow Run Airport Ypsilanti, Michigan
1	Attn: Librarian Via: ONR

No. of Copies	
	APL/JHU 8621 Georgia Avenue Silver Spring, Maryland
2	Attn: Tech. Rpts. Group Via: InsOrd
	The Ohio State University Research Foundation Nineteenth Avenue Columbus 10, Ohio
1	Attn: Security Officer Via: ONR
	CIT Pasadena 4, California
1	Attn: Aeronautics Dept.
2	Attn: Jet Propulsion Lab. Via: ONR
	University of Minnesota Minneapolis 14, Minnesota
1	Attn: Mechanical Eng. Dept. Via: ONR
1	BAR Aeroject-General Corporation 6352 N. Irwindale Ave. Azusa, California
	RAND Corp. 1700 Main St. Santa Monica, California
1	Attn: Lib., USAF Project RAND Via: InsMat
	Douglas Aircraft Co., Inc. Santa Monica Division 3000 Ocean Park Blvd. Santa Monica, California
1	Attn: Chief Engineer Via: InsMat
1	CONVAIR Corp. A Div. of Gen. Dynamics Corp. Daingerfield, Texas Via: InsMat

No. of Copies		No. of Copies	
1	United Aircraft Corporation 400 Main Street East Hartford 8, Connecticut Attn: Chief Librarian Via: InsMat	2	Eastman Kodak Company Navy Ordnance Division 50 West Main Street Rochester 14, New York Attn: Mr. W. B. Forman Via: InsOrd
1	Guggenheim Aeronautical Lab. California Inst. of Technology Pasadena 4, California Attn: Aeronautics Lib. Via: ONR		
1	Cornell Aeronautical Lab., Inc. P. O. Box 235, 4455 Genessee St. Buffalo 21, New York Attn: Librarian Via: InsMat		
1	Lewis Flight Propulsion Lab. 21000 Brookpark Road Cleveland 11, Ohio Attn: Chief, Supersonic Propulsion Div. Via: InsMat		
2	Armour Research Foundation 10 West 35th Street Chicago 16, Illinois Attn: Dept. M Via: InsMat		
1	Hughes Aircraft Corp. Culver City, California Attn: Assistant Director GMRD Div. Via: InsMat		
1	McDonnell Aircraft Corporation P. O. Box 516 St. Louis 3, Missouri Via: InsMat		
1	General Electric Company 2900 Campbell Avenue Schenectady 5, New York Attn: Library, Guided Missiles Dept. Via: InsMat		

Aeroballistic Research Department
External Distribution List for Aeroballistic Research (X 1a)

No. of Copies	
1	Chief, Fluid Mechanics Section National Bureau of Standards Washington 25, D. C.
	National Bureau of Standards Washington 25, D. C.
1	Attn: Applied Math. Div.
1	Commanding Officer Office of Naval Research Br. Off. Box 39, Navy 100 Fleet Post Office New York, New York
	Langley Aeronautical Laboratory Langley Field, Virginia
1	Attn: Theoretical Aerodynam. Div.
	Case Institute of Technology Cleveland 6, Ohio
1	Attn: G. Kuerti
	Massachusetts Institute of Tech. Cambridge 39, Mass.
1	Attn: Prof. Joseph Kaye Room 1-212
	The Johns Hopkins Univ. Charles and 34th Streets Baltimore 18, Maryland
1	Attn: Dr. Francis H. Clauser
2	Director Inst. for Fluid Dynamics and Applied Mathematics University of Maryland College Park, Maryland
	Cornell University Graduate School of Aero. Eng. Ithaca, New York
1	Attn: Prof. W. R. Sears
1	AERCON, Inc. 560 Punahou St. Altadena, California
	Princeton University James Forrestal Research Center Gas Dynamics Laboratory Princeton, New Jersey
1	Attn: Prof. S. M. Bogdonoff

No. of Copies	
	Commanding Officer and Director
	David Taylor Model Basin
	Washington 7, D. C.
2	Attn: Hydrodynamics Lab.
	Res. and Development Board
	Pentagon 3D1041
	Washington 25, D. C.
2	Attn: Library Branch
	Jet Propulsion Lab.
	CIT
	4800 Oak Grove Drive
	Pasadena, California
1	Attn: F. E. Goddard, Jr.
1	Attn: Dr. P. P. Wegener
1	Attn: Mr. J. Laufer
1	Attn: Mr. D. R. Bartz
1	Attn: Mr. L. Lees
1	Attn: Prof. M. S. Plesset
1	Attn: Dr. H. W. Liepmann
1	Attn: Mr. A. Roshko
1	Attn: Dr. D. Coles
1	Attn: Mr. Satish Dhawan
	University of Illinois
	202 E. E. R. L.
	Urbana, Illinois
1	Attn: Prof. A. H. Taub
	MIT
	Cambridge 39, Massachusetts
1	Attn: Project Meteor
1	Attn: Prof. G. Stever
1	Attn: Prof. Dean
1	Attn: Mr. J. Baron
1	Attn: Mr. M. Sweeney, Jr.
1	Attn: Prof. E. Reissner
1	Attn: Guided Missiles Library
	Bureau of Ordnance
	Room 0432, ReS1-e
	Main Navy Building
	17th St., & Const. Ave.
	Washington 25, D. C.
1	Attn: Mr. L. L. Liccini

No. of Copies	
	New York University
	45 Fourth Avenue
	New York 3, New York
1	Attn: Prof. R. Courant
	Polytechnic Institute of Brooklyn
	527 Atlantic Avenue
	Freeport, New York
1	Attn: Dr. A. Ferri
1	Attn: Prof. N. J. Hoff
1	Attn: Dr. M. Bloom
1	Attn: Dr. P. Libby
	AeroJet--General Corp.
	6352 North Irwindale Ave.
	Axusa, California
1	Attn: BuAer Representative
	Harvard University
	Cambridge 38, Massachusetts
1	Attn: Prof. G. Birkhoff
1	Attn: Prof. R. von Mises
	Hughes Aircraft Co.
	Missile Aero. Dept.
	Culver City, California
1	Attn: Dr. Allen E. Puckett
	Engineering Res. Institute
	East Engineering Bldg.
	Ann Arbor, Michigan
1	Attn: Dir. of Icing Res.
	The Artillery School
	Anti-Aircraft & Guided Missiles Branch
	Fort Bliss, Texas
1	Attn: Res. & Analysis Sec.
	Brown University
	Div. of Engr.
	Providence, Rhode Island
1	Attn: Prof. R. F. Probstein

No. of Copies	
	Arnold Res. Organization, Inc. Chief, Gas Dynamics Facility Tullahoma, Tennessee
1	Attn: Mr. R. Smelt
	Facilities Division DCS/ Development Hdqts. USAF, Rm. 5C368 Pentagon Washington 25, D. C.
1	Attn: Dr. F. L. Wattendorf
	Ohio State University Aero. Engr. Department Columbus, Ohio
1	Attn: Prof. G. L. Von Eschen
	Consolidated Vultee Aircraft Corp. San Diego, California
1	Attn: Mr. R. L. Bayless
	University of Minnesota Minneapolis 14, Minnesota
1	Attn: Dr. E. R. G. Eckert
1	Attn: Dr. W. S. Bradfield
1	Attn: Dr. J. Hartnett
	Holloman Air Force Base Alamagordo, New Mexico
1	Attn: Dr. G. R. Eber
	Air Force Dir. of Res. & Development Pentagon, Rm. 4E348 Washington 25, D. C.
1	Attn: Dr. A. E. Lombard
	North American Aviation Inc. Aerophysics Lab. Downing, California
1	Attn: Dr. E. R. Van Driest
	Douglas Aircraft Co., Inc. El Segundo, California
1	Attn: D. N. Morris
1	Attn: K. E. Van Every

No. of Copies	
	Daniel Guggenheim School of Aeronautics New York University New York 3, New York
1	Attn: Prof. H. F. Ludloff
	U. S. Air Force Main Navy Bldg., Rm. 3816 Washington 25, D. C.
1	Attn: Major H. W. Keller
	University of California P. O. Box 1663 Los Alamos, New Mexico
1	Attn: W. F. Brown
	Applied Physics Laboratory The Johns Hopkins University 8621 Georgia Avenue Silver Spring, Maryland
1	Attn: Dr. F. Frenkiel
1	Attn: Dr. F. K. Hill
1	Attn: Mr. E. A. Bonney
1	Attn: Mr. D. Fox
	Chance-Vought Aircraft Development Section Dallas, Texas
1	Attn: Dr. R. E. Wilson
1	Dept. of Aeronautical Engr. Rensselaer Polytechnic Institute Troy, New York
	AVION - Division of ACF Paramus, New Jersey
1	Attn: Mr. R. G. Grape
	Philco Corporation G & I Division-Research 4700 Wissahickon Ave. Philadelphia 44, Penn.
1	Attn: Mr. A. Bernstein
	Research Dept. United Aircraft Corp. East Hartford, Connecticut
1	Attn: Mr. W. E. Powers

No. of Copies	
	Air Force Armament Center Eglin Air Force Base, Florida
1	Attn: ACZ
	General Electric Company Special Defense Projects Dept. 3198 Chestnut Street Philadelphia, Pennsylvania
1	Attn: Dr. Nathan Ness
	CONVAIR A Division of General Dynamics Corp. Scientific Research Laboratory 3595 Frontier Street San Diego, California
1	Attn: Mr. M. Sibulkin
1	University of Southern California Engineering Center 3518 University Ave. Los Angeles 7, California
1	Avco Manufacturing Corp. Research Labs 2385 Revere Beach Parkway Everett 49, Massachusetts Via: WDSIT Western Dev. Div. Inglewood, Calif.